Clouds and the Earth's Radiant Energy System (CERES)

Validation Plan

GEOLOCATE AND CALIBRATE EARTH RADIANCES INSTRUMENT

(SUBSYSTEM 1.0)

Robert B. Lee, III[1], Kory J. Priestley[1], and Richard N. Green[1]

[1]Atmospheric Sciences Competency, NASA Langley Research Center, Hampton, VA. 23681-0001

Release 4.0
August 2000

CERES GEOLOCATE AND CALIBRATE EARTH RADIANCES
LEVEL 1 INSTRUMENT VALIDATION PLAN

1.1 INTRODUCTION

This plan is designed to (1) trace the absolute calibrations of the Clouds and the Earth's Radiant Energy System (CERES) spacecraft sensors radiance and geometric measurements from ground to flight, (2) define short-term and long-term shifts or drifts in the measurements caused by sensor response variations, and (3) determine CERES measurement consistency among the same types of CERES sensors on the same and different spacecraft platforms and with other similar spacecraft radiance/flux measuring sensors. The plan and on-orbit results are described in detail by Lee *et al.* (1996a, 1998) and Priestley *et al.* (2000)

1.1.1 Measurement and Science Objectives

The CERES sensors are scanning thermistor bolometers which measure Earth-reflected and Earth-emitted filtered radiances in the broadband shortwave (0.3 µm - 5.0 µm), broadband total-wave (0.3 µm - >100 µm), and narrow-band water vapor window (8 µm-12 µm) spectral regions. Broadband longwave radiances (5 µm - >100 µm) are derived from the differences between the total-wave and shortwave radiances. These radiance measurements, along with imager measurements, define the impacts of clouds and of certain cloud properties upon the Earth's radiation budget and climate (Wielicki and Barkstrom 1991, Wielicki *et al.* 1996, Wielicki *et al.* 1998).

1.1.2 Missions

On November 27, 1997, the first set of the CERES bolometers was placed into orbit aboard the Tropical Rainfall Measuring Mission (TRMM) Spacecraft platform. The TRMM spacecraft was launched into a low-inclination 35°, 350-km altitude orbit using a National Space Development Agency (NASDA) H-II expendable launch vehicle from the Tanegashima Space Center, Japan. During December 1999, the second and third sets of bolometers are scheduled for launch on the EOS Terra spacecraft platform. December 2000, the fourth and fifth sets of bolometers will be launched on the EOS Aqu spacecraft. The EOS spacecraft platforms will be launched into Sun-synchronous polar, 705-km orbits using NASA Atlas IIC launch vehicles.

1.1.3 Science Data Product

The level 1, CERES instrument data product is geolocated filtered broadband Earth radiances, in $Wm^{-2}sr^{-1}$, at the top-of-the-atmosphere (~30 km). For average target scenes less than 100 $Wm^{-2}sr^{-1}$, the broadband shortwave and longwave instrument measurement accuracy requirements are 0.8 $Wm^{-2}sr^{-1}$ and 0.6 $Wm^{-2}sr^{-1}$, respectively, as indicated in Table 1. Earth Radiation Budget Experiment (ERBE) Spacecraft (Barkstrom 1984, Barkstrom and Smith 1986) in-flight calibration systems, earlier versions of the CERES systems, were used to verify shortwave and longwave radiance measurement precisions at the $\pm$ 0.3% measurement precision levels (Lee *et al.* 1993). During the ERBE missions, a coastline validation technique (Hoffmann *et al.* 1987) was used to verify geolocation calculations at the $\pm$ 6 km uncertainty level. The coastline technique was improved and used to validate the TRMM CERES geolocation calculations at uncertainty

levels approaching $\pm$ 0.5 km near the nadir (Currey *et al.* 1998).

1.2 VALIDATION CRITERION

1.2.1 Overall approach

The CERES level 1 radiometric data product validation plan includes assessments of (1) the degree to which the absolute longwave and shortwave radiometric scales are transferred from the ground to space by the CERES sensors and in-flight calibration sources; (2) the in-flight long-term stabilities of the CERES sensor responses; (3), in the case of sensor response drifts or shifts, revisions to the sensor in-flight count conversion coefficients (gains and offsets); and (4) validations of the geolocation calculations from analyses of the calculated locations of geometric registration sites and their corresponding measured filtered radiances. Ground-calibrated instrument count conversion coefficients are used to convert the sensor output signals into radiances. The Ground coefficients were derived in the TRW Radiometric Calibration Facility (Lee *et al.* 1996b, Lee *et al.* 1997, Lee *et al.* 1998) and tied radiometrically to the International Temperature Scale of 1990 (ITS-90). The ground-derived coefficients are revised only if the sensor response drifts or shifts more than 0.5 $Wm^{-2}sr^{-1}$ in the longwave spectral region or more than 0.8 $Wm^{-2}sr^{-1}$ in the shortwave region. If the sensor response drifts or shifts above these levels, the flight coefficients will be revised off-line in science computing facilities (SCF) and applied only after the approval of the CERES Science Team. The TRMM/CERES ground-derived gains and offsets were used to process the December 1997 thru June 2000 flight measurements. Analyses of ground and flight calibrations indicated that the CERES bolometers' responses (gains) did not change between the ground and the on-orbit calibrations and that they were stable at uncertainty levels better than 0.2 $Wm^{-2}sr^{-1}$. Therefore, the ground-derived gains were not revised. Radiometric measurements of deep space were used to define the final sensor zero-radiance offsets. Therefore, the archived January thru June 2000 radiances were processed using the ground gains and on-orbit offsets.

The elements of the overall validation plan for the level 1 geolocated filtered radiances include (a) radiometric analyses (Lee *et al.* 1992, Lee *et al.* 1993, Lee *et al.* 1998) of ground and on-orbit/in-flight calibration measurements; (b) geometric registration sites/coastline detection analyses (Hoffmann *et al.* 1987, Currey *et al.* 1998) to estimate upper limits in geolocation errors; and (c) single and multi-spacecraft intercomparisons of Earth radiance measurements from the same type of broadband sensors (Avis *et al.* 1994, Green and Avis 1996) in the cross-track and rotating azimuth plane (RAP) Earth radiance scanning modes.

The CERES instrument radiometric performance is validated/checked using multi-sensor comparisons of Earth radiance measurements from the same spacecraft (Green and Avis 1996) and from other past and current spacecraft sensors [Earth Radiation Budget Satellite (ERBS) nonscanners, ERBS scanners, Scanner for Radiation Budget (ScaRaB) scanners, etc.). Using in-flight calibration sources, the CERES sensors were checked for instrumental drifts or shifts. These activities, may not guarantee that the CERES data are consistent with the historical ERBS data (Barkstrom 1984, Barkstrom and Smith 1986), or that the in-flight calibration systems are stable. For example, if on the ground, the total channel is tested against the on-board blackbodies. In flight, if the same procedure is performed, and if the two readings are different, it will not be clear whether the difference is caused by the radiometer or by the blackbody. The same is true for any detected

drift. For these reasons, the CERES radiances are validated against Earth validation targets (Staylor 1986, 1993, Priestley 2000). The statistics of the radiance for these targets were established with 5 years of validated ERBS scanner data (Green and Avis 1996). If statistically significant differences between the CERES measurements and the Earth validation targets are found, and if these differences are consistent with the in-flight calibration systems and results are within the uncertainties of the instrument calibration and validation, then the radiances will be revised with the approval of the CERES Science Team. If the differences are outside the instrument uncertainties, then all analyses will be re-examined and additional sources of verification will be sought. It is probable that superior CERES calibration systems and consistency between the CERES ground and in-flight calibration will make CERES the standard and assess possible biases in the ERBS data.

1.2.2 Sampling Requirements and Trade-offs

For a minimum of the first 30 days in orbit, the sensor contamination doors are closed. During this period, the sensors are calibrated daily using measurements from the internal calibration module (ICM) which are referenced to the radiances from the contamination doors' emitted and reflected radiances. After the doors are opened, measurements of the ICM sources are performed daily during the first week, every other day during the second week, once a week during the third and fourth weeks, and thereafter every 14 days (Lee *et al.* 1998).

Validation measurements of the Earth radiances are used to verify sensor response changes, indicated by in-flight calibrations. The CERES science team will conduct detailed analyses of at least the first 6 months of in-flight calibrations and validations before the sensor gains or offsets are revised. Validation of the CERES radiances against Earth validation targets require a minimum of two months of data. Additional months will strengthen the statistical hypothesis tests and increase the probability of detecting errors if they exist. After the 90th day and during the remainder of the mission, the in-flight calibrations and validation studies will be evaluated every 14 days to detect short-term and long-term sensor relative responses changes. The CERES sensors sampling rate of Earth radiances are sufficient to carry out planned validation studies.

1.2.3 Measures of Success

The CERES calibration/validation efforts will be partially successful if the CERES mean annual global unfiltered longwave radiances are approximately 77 ± 2 $Wm^{-2}sr^{-1}$ over an integral number of spacecraft precession cycle. During the 1985-1986 period, the precessing Earth Radiation Budget Satellite (ERBS) and the polar-orbiting NOAA-9 spacecraft scanning narrow-field-of-view thermistor bolometer sensors yielded global mean Earth radiance values near 77 $Wm^{-2}sr^{-1}$. During the 1984-1998 period, Earth irradiance measurement trends from the ERBS nonscanning wide-field-of-view (WFOV) active-cavity radiometers indicate that the annual mean global Earth longwave radiances varied less than 2 $Wm^{-2}sr^{-1}$ from the 77 $Wm^{-2}sr^{-1}$ value (Rutan *et al*. 1999, Bush *et al.* 1999). Shortwave radiances vary with the local solar time of the measurements. Therefore, for the shortwave radiances, the measures of success cannot be define as precisely as the measures for the longwave radiances.

The January-February 1998, TRMM/CERES longwave and shortwave Earth radiances were found

to be within 0.5 Wm^{-2}sr^{-1} of the corresponding inferred January-February 1998, ERBS nonscanner Earth radiances (fluxes divided by π). The April-August 1998 radiance comparisons will be performed when the ERBS measurements are reduced. The processing of the April-August 1998, ERBS data was delayed due to difficulties in reading the recently revised spacecraft telemetry. No ERBS measurements were obtained during March 1998.

The measure of successful validation of the CERES radiances is the statistical agreement between the instrument on-board validation plan and the empirical validation plan such that there are no additional statistically significant adjustments to the radiances. In addition, it must be shown that any error large enough to invalidate the radiances would have been detected. This measure of validity and the mission accuracy goals will dictate how many months of data is required to reach this decision.

1.3 PRE-LAUNCH ALGORITHM TESTS/DEVELOPMENT ACTIVITIES

1.3.1 Field Experiments and Studies

Further studies are needed to insure that the CERES total channel radiances at night, which are taken as the absolute reference, are statistically consistent with established data sets.

1.3.2 Operational surface Networks

N/A

1.3.3 Existing Satellite Data

1.3.3.1 Validation of the longwave response of the total channel - The longwave response of the total channel and the individual offsets for each distinct measurement position are validated by comparing data averages to an Earth validation target with known radiance statistics. A good longwave validation target is the Tropical Mean (TM) or all tropical ocean between $\pm 20^{o}$ latitude with any cloud condition. From 5 years of validated ERBS scanner data, we know that a single radiance measurement over tropical ocean at a given viewing zenith angle varies by 15% (one standard deviation), and that the daily average of all measurements over the tropical ocean at the same viewing zenith varies by 1.2%.The monthly average varies by 0.6%.Thus, averaging 30 days of data only reduces the uncertainty from 1.2% to 0.6% and implies that daily averages are not independent. However, we have determined that the uncertainty is reduced by $\sigma_{\bar{x}} = \sigma_x / \sqrt{n^{0.62}}$ where σ_x is the uncertainty (standard deviation) of one month, and $\sigma_{\bar{x}}$ is the uncertainty of n months. Knowing the statistics of the Earth validation targets allows us to detect statistically significant errors in the longwave response of the total channel.

CERES nadir radiances from the total channel at night are averaged over the tropical ocean for each month and the average of all months is recorded. For the five years (or 60 months) of ERBS data we have the TM is 87.13±0.14 Wm^{-2}sr^{-1}. For the eight months of CERES-TRMM from January to February, 1998 we have TM equal to 89.13±0.23 Wm^{-2}sr^{-1}. The equivalent eight month

average for ERBS is 87.22±0.16 Wm^{-2}sr^{-1} and the TMs are statistically different implying an instrument error. However, the TM for CERES-TRMM for March, 2000 is not statistically different from ERBS. These TM results and other data has led us to conclude that the tropics during the 1998 El Nino period were warmer than usual and that the CERES-TRMM longwave radiance from the total channel is not in error. This method of validation will also be applied to CERES on Terra and Aqua.

The TM can also be calculated not only at nadir but at all scan positions to validate the individual scan dependent offsets. Four sources that cause offset errors are (1) electronic noise, (2) space clamp errors, (3) 2nd time constant errors, and (4) elevation or flex errors. Let us divide the 660 scan positions into four segments denoted A, B, C, and D. Segment A is from the initial space view (scan position #1) to the first nadir (#168). Segment B is from #168 to #330, etc. Electronic noise will not show in the TM because we average many data points. If we calculate the TMs for each position in A, B, C, and D, then a plot of the TM differences for (A-D) and (B-C) give an indication of space clamp and 2nd time constant errors. For CERES data we have found the flex errors dominate. These errors result from the rotation of the scan head from its original start position to its furthest position on the opposite side of the spacecraft. Now, segments A and C scan from space to nadir and are affected by the 2nd time constant. Segments B and C are affected by flex errors. Only segment D is free of these errors. Thus, we can determine offset errors by fitting a smooth curve through the TMs for segment D and use this curve as a reference from which to determine offsets for A, B, C, and D. This procedure was followed to validate the CERES-TRMM offsets for the total and window channels and will be applied to CERES on Terra and Aqua.

1.3.3.2 Validation of the window channel - A line-by-line theoretical radiative transfer code is used to validate the response of the window channel for specific earth scenes (Kratz and Rose, 1999, Kratz et. al. 2000). The window channel radiances are validated in the same way as the longwave radiances of the total channel (Section 1.3.3.1). The only difference is the addition of a narrowband to broadband conversion which will increase the uncertainty in the statistical tests.

1.3.3.3 Validation of the shortwave channel and the shortwave part of the total channel - The shortwave channel is validated by a three channel intercomparison test (Green and Avis 1996) and shortwave Earth validation targets. The three channel test is based on the redundancy between the shortwave, total, and window channel measurements. Since shortwave radiances are highly variable, it is advantageous to examine daytime longwave differences and infer shortwave differences.

The first step of intercomparing the three channels is to regress the window channel against the validated total channel at night. Having matched the window radiances to the longwave radiances of the total radiances, we use the window channel to transfer our longwave standard from nighttime to daytime. We determine the daytime longwave radiances from the window channel and also determine the longwave radiances by the normal approach of subtracting the shortwave from the total channel radiances. These two estimates of broadband longwave radiance should agree on average. Recall that the longwave portion of the total channel radiances has been validated and the window radiances matched to the total at night. Only shortwave errors would cause the two longwave measurements to differ on average. Thus, if there is a significant difference between the longwave radiances and those from the matched window channel and the total minus shortwave channel, then either the shortwave channel is in error, or the shortwave part of the total channel is

in error, or both are in error. We cannot determine where the shortwave error source is located from the three channel intercomparison test.

Next, we examine shortwave Earth validation targets with known statistics from validated ERBS data. Likely target areas are deep convective clouds (Currey *et al.*, 1999)and the desert area known as the Arabian Empty Quarter within the Saudi Desert. This desert area is almost entirely sand dunes and sand seas, and the lack of moisture and the saline nature of the sand cause it to be virtually free of all vegetation (Staylor 1986). As a result this area is uniform in shortwave. We then compare the shortwave channel measurements against the shortwave validation target and test for statistically significant differences. We can also test the shortwave portion of the total channel against these targets by subtracting the matched window channel from the total channel. These tests will be used to proportion the shortwave gain change as inferred from the three channel Intercomparison test between the two potential shortwave error sources.

The three channel intercomparison test for CERES-TRMM showed a difference in the daytime longwave Tropical Mean from the window channel and from the total and shortwave channels. This difference implied a 1.2% shortwave error. An analysis of deep convective clouds implied a 0.7% shortwave error. These errors were traced back to slight errors in the model of the spectral response of the shortwave channel and the shortwave part of the total channel. These model errors were corrected and new spectral correction coefficients were calculated (Loeb *et. al*, 2000).

1.3.4 In-flight Calibration Systems

The ground derived count conversion coefficients (gains and offsets) are used as the preliminary flight sensor count conversion coefficients. Using built-in flight calibration systems, sensor calibrations were conducted during the ground derivations of the coefficients; during the thermal-vacuum testing of the sensors on the spacecraft, prior to launch; and shortly after launch. Analyses of the ground to launch flight calibration measurements defined the degree to which the sensor and flight calibration systems transferred the longwave and shortwave absolute radiometric scales into orbit. After launch, analyses of the time series of the in-flight calibrations define whether revisions to the initial in-flight coefficients are necessary along with analyses of validation plan elements.

1.3.4.1 - CERES Instrument Package - Each CERES instrument package consists of a scanning thermistor bolometer sensor assembly (Lee *et al.* 1996b), elevation axis drive system, azimuth axis drive system, pedestal, and associated electronics as shown in Fig. 1. The CERES instruments were designed, manufactured, and tested by TRW's Space and Electronics Group, Spacecraft and Technology Division (Redondo Beach, CA) under NASA contract NAS1-19039. Each sensor assembly has three sensor units. One is a broadband shortwave unit which measures Earth-reflected solar radiances in the 0.3 µm to 5.0 µm spectral region. The second sensor unit is a total-wave broadband radiometer which measures both Earth-reflected solar and Earth-emitted longwave radiances in the 0.3 µm to >100 µm spectral region. The third one is a narrow-band unit which measures Earth-emitted longwave radiances in the 8 µm to 12 µm spectral region. The three sensors are co-aligned and mounted on a spindle that scans about the elevation axis (See Figs. 1 and 2). The sensor assembly elevation pointing can be resolved at the 0.005 degree level using 16 bit optical position encoders. The sensors fields' of view overlap by at least 98%. The sensors and elevation axis drive system can rotate about the azimuth axis at rates between 4 and 6 angular

degrees per second of time. The azimuthal pointing can be resolved at the 0.005 degree level using position encoders. Once every 10 milliseconds, the averaged elevation and azimuth positions are sampled and recorded. The mass of each instrument package is less than 50 kg. When the azimuth drive is stationary and when the sensor scans in the elevation plane (cross track mode), each instrument package uses less than 41 Watts of electrical power. Each instrument uses less than 47 Watts in the biaxial mode, in which the instrument is both scanning in the elevation plane and rotating in the azimuthal plane (rotating azimuth plane mode). The instrument package can be contained in a cube, 60 cm in height.

The Earth radiance measurements are collected in the normal or short science scan cycle. All science and calibration scan cycles are 6.6 seconds in duration in which the sensors output signals are sampled every 10 milliseconds while housekeeping data are sampled, at least once. In Fig.2, a cross-sectional view of the CERES instrument is presented for the elevation plane. For the TRMM orbital configuration, the normal scan cycle included observations of cold space [near zero radiance source at a temperature of 2.7 K (Turner 1993)] at the elevation angle of 11 degrees, of the Earth between 19 and 161 degrees, a second look at cold space on the other side of the Earth at 169 degrees, and of the built-in internal calibration module (ICM) system at 194 degrees. For the EOS orbit, cold space will be observed at the elevation angles of 18 and 162 degrees while the Earth is observed between 26 and 154 degrees. During normal science cycle, the internal calibration sources are not activated. As shown in Fig. 2, in the short scan, the TRMM/CERES sensors observe cold space at 11 degrees, and Earth between 19 and 141 degrees. During short scans, observations are not conducted of the cold space at 169 degrees and of the calibration system at 194 degrees. The short scan will be used primarily during the rotating azimuth plane (RAP) operations to prevent the sensors from staring at the Sun and the solar observations altering the sensors' responses. The short scan restricts the scanning sensors to elevation angles below the Earth limb on the Sun side.

The first cold space observations, at the elevation angle of 11 degrees, are used in the data reduction process for each 6.6 second scan cycle. The set of space observations, at 169 degrees, are not used in the data processing because they are not available during the short scans.

The cross-track mode is the most important operational science measurement configuration in which the azimuth position is fixed. The sensors operate in normal or short scan cycles in a whiskbroom pattern perpendicular to the orbital plane. The cross-track measurements are the primary data used by the CERES science team for performing Earth radiation budget studies.

The rotating azimuth plane (RAP) mode is an operation in which the azimuth axis is rotated at a constant rate of 6 angular degrees per second in one direction for 30 seconds and then it is rotated in the opposite direction at the constant 6 degrees per second rate for the next 30 seconds. A complete azimuth scan cycle is completed in 1 minute. In the RAP mode, the elevation plane of the sensors oscillates through an azimuth angle of 180°. The short scan cycle is used to avoid possible observations of the Sun near the sunrise or sunset positions. During the RAP operations, the sensors can measure radiances from geographical scenes with varying incident solar radiation and observing geometry. The RAP data will be used to compute new angular distribution models for converting sensor radiances into irradiances at the top of the atmosphere.

During the TRMM mission, the CERES instrument package operated on a three-day cycle, in which the instrument scanned in the cross-track configuration for two consecutive days, and on the third day, scanned in the RAP configuration. During the EOS AM- mission, there will be two instrument packages. During the 30-60 day period after launch, both EOS AM-1 instruments will be operated on three-day cycles. On the first day of the cycle, each instrument will operate in the cross-track configuration. On the second day, one instrument will operate in the RAP configurations while the other will operate in the cross-track mode. On the third day, the operating configurations will be reversed for the two instruments. After the 90 day, one instrument will operate only in the cross-track mode while the other instrument will operate in the RAP mode. Every 28th day, both instruments will operate in the cross-track configurations in order to compare their radiometric productions instantaneously over the same geographical locations.

1.3.4.2 Sensor Unit - Each sensor unit consists of a telescope baffle, Cassegrainian telescope, and thermistor bolometer detector module. The unit is 9.2 cm in length. The telescope baffle prevents energy from striking the active bolometer flake at angles greater than 16° off of the telescope optical axis. The f/1.8 Cassegrainian telescope module has an 18-mm diameter silvered primary mirror and a silvered secondary mirror. In the shortwave and in the water vapor window sensor units, filters are located in two places: before the secondary mirror spider and in front of the active bolometer flake. The 8-µm to 12-µm window filter system consists of a 1-mm thick zinc sulfide and a 0.5-mm thick cadmium telluride filter element. Each shortwave filter is a 1-mm thick fused, waterless quartz element. The total-wave sensor unit does not have an optical filter.

The detector module has an active and a reference thermistor bolometer flake with time constants less than 9 and 12 milliseconds, respectively. The TRMM (proto-flight model) shortwave, total-wave, and window active flakes have time constants of 8.7, 7.9, and 8.2 milliseconds. In the detector module, the active and the reference flakes are mounted on separate disk assemblies which are in thermal contact with each other and with the heatsink which is maintained at a constant temperature of 38° Celsius using a 2.3-Watt electrical heater. The active and reference flakes are covered with 12-µm thick absorptive black paint layers of Aeroglaze Z-306 doped with 10% carbon black. The absorptance of the paint layer is greater than 85% out to 100 µm (Jarecke *et al*. 1991).

1.3.4.3 Flight Algorithms - The CERES data reduction algorithms follow the procedures developed for the NASA Earth Radiation Budget Experiment (ERBE) to preserve continuity with the ERBE long-term data sets. The filtered radiance measured by each sensor unit can be expressed by following algorithm (Halyo et al. 1989, Lee et al. 1989, Lee *et al*. 1996b, Lee *et al*. 1998).

$$\tilde{L}(t-\tau) = G_V[m(t) - \bar{m}(t_k) - o(t)] + \frac{t - t_k}{\Delta t}[G_S(\bar{m}(t_{k+1}) - \bar{m}(t_k))$$

$$+ G_H(T_H(t_{k+1}) - T_H(t_k)) + G_D(V_D(t_{k+1}) - V_D(t_k)) \tag{1}$$

$$+ G_B(V_{bias}(t_{k+1}) - V_{bias}(t_k))]$$

where

$$t_k = t_{k-1} + \Delta t$$

and $m(t)$ = instrument output (digital counts) sample at time t, $\overline{m}\,(t_k)$ is the averaged instrument output in digital counts when viewing cold space at t_k at the beginning of every 6.6 second scan, and $o\,(t)$ is the sensor zero-radiance offset variation with elevation angle/geometry. The other terms and constants are defined as

$T_H(t_k)$ = heat sink temperature measurement (K) at t or most recent time
Δt = total scan period of 6.6 seconds.
t_k = time at end of space look (sec.)
t = sampling instant (sec.)
$V_{bias}(t)$ = sensor bridge bias voltage measurement at time t or most recent value, counts
$V_D(t_k)$ = drift balance digital to analog converter (DAC) voltage measurement at time t
                  or most recent value, counts
τ = average time lag between the instantaneous detector optical field of view and point
                  spread function centroid (sec.).
C = digital to analog conversion factor, 409.5 digital counts/volt

while the coefficient gain terms A_V, A_S, A_H, A_D, and A_B are defined as:

$$G_V = \frac{AV}{CV_{bias}(t)} \tag{2}$$

$$G_S = \frac{AVA}{CV_{bias}(t)} \tag{3}$$

$$G_H = \frac{AHA}{CV_{bias}(t)} \tag{4}$$

$$G_D = \frac{AD}{CV_{bias}(t)} \tag{5}$$

$$G_B = \frac{AB}{CV_{bias}(t)} \tag{6}$$

where AV, AVA, AHA, AD, and AB are constants determined using the ground calibration data (Lee *et al.* 1996b; Jarecke *et al.* 1993) and where C is equal to 409.5 digital counts per volt.

The housekeeping data $T_H(t_k)$ and $V_D(t_k)$ are transmitted to Earth once every scan and are not available for every instrument output sample during the scan. The sensor gain term, G_V, in (1) is the most important gain term. It is important to point out that the G_H, G_D, and G_B terms in CERES

thermistor bolometer ground calibration data analyses were found to be negligible and set equal to zero.

In Eq. (1), the sensor calibration gain, G_V, is the most important term. The remaining terms have relatively small impacts upon the calculated filtered radiances. G_S is equal in magnitude to G_V, but opposite in sign [AVA = -AV]. During the CERES sensor ground calibrations, V_{bias}, T_H, and V_D were essentially constant. Consequently, values of AB, AHA, and AD were equated to zero, setting the G_H, G_D, and G_B terms equal to zero.

The sensor's response functions contain a slowl transiene at the 1% level (Smith *et al.* 2000). Modeling studies show that the transient is caused by the conduction of heat from the active bolometer to the compensator bolometer. For the PFM total sensor, the single thermal mode time constant was 345 milliseconds. In the data processing system, a numerical filter is used to account for the transient. Since the transient consists of a single slow mode, its response, v(t), can be computed at time t in terms of its previous level. The sensor output voltage, m(t), can be characterized by the following recursive equation

$$v(t) = p_0 v(t- dt) - p_1 m(t) \tag{7}$$

The slow mode is subtracted from the sensor output voltage to yield the transient corrected sensor output voltage u(t) as

$$u(t) = m[(t) - v(t)] \, (1+c) \tag{8}$$

The filter weights p_0 and p_1 are given by

$$p_0 = \exp \, [(-\lambda dt)(1 + c)] \tag{9}$$

$$p_1 = c \, (1 - p_0) \, / \, (1 + c) \tag{10}$$

where $1/\lambda$ is equal to the characteristic time of the slow mode and c is the response of the slow mode to a unit step input. The constants "λ" and "c" are determined from calibration data.

1.3.4.4 In-Flight Calibration Systems - The internal calibration module (ICM) and the mirror mosaic attenuator (MAM) are the two in-flight systems which are built into the CERES instrument package and are used to define shifts or drifts in the sensor responses. The location of the in-flight calibration systems are shown in Fig. 2, at the elevation angle of 194 degrees. The primary in-flight calibration system is called the internal calibration module (ICM). The ICM and the sensors will carry the ground calibration radiometric scale into orbit. As shown in Fig. 3, The ICM consists of 2.75-cm diameter, concentric grooved, anodized black aluminum blackbody sources for the total and window sensors, and an evacuated tungsten lamp source, known as the shortwave internal calibration source (SWICS), for the shortwave sensor. The CERES SWICS operates at 4 constant specific radiance levels, including off, between 0 and 400 $Wm^{-2}sr^{-1}$. ICM's were used to calibrate thermistor bolometers and active-cavity radiometers aboard the Earth Radiation Budget Satellite (ERBS), NOAA-9, and NOAA-10 spacecraft platforms. The TRMM/CERES SWICS's operated at levels near of 0.3, 81.4, 237.2, and 366.0 $Wm^{-2}sr^{-1}$.

In ground vacuum facilities, the CERES blackbodies were operated and maintained at three temperatures between ambient and 320 K. Imbedded in the blackbodies, platinum resistance thermometers (PRT) indicate the temperatures of the blackbodies' emitting surfaces. Before the PRT's are placed in the ICM blackbody structure, the PRT's are calibrated in a temperature controlled bath to verify that the correct coefficients are used in the PRT temperature equation at 273.16 K.The blackbody radiances are calculated from the Stefan-Boltzman relationship using the PRT temperatures and the effective blackbody emittances. Using (1) above, the total-wave and window sensors measurements of the in-flight blackbodies are converted into filtered radiances. The calculated sensor and the calculated blackbody radiances are compared using regression analyses to verify that the blackbodies were on the same radiometric scale as the sensors. On-orbit, the CERES blackbodies operate at the three different, constant temperature levels of ambient, 32 K, and 52 K. However, the ERBE in-flight blackbodies operated from ambient temperature (291 K thru 303 K) to 20 degrees above the ambient temperature. The ICM calibrations were performed when the sensors operate in the normal scan cycle. The SWICS was not operated at the same time that the blackbody heaters were turned off.

In Fig. 4, the ERBS ICM flight calibration measurements demonstrate that the ERBS sensor bolometers and their calibration sources were stable within 0.3% over a 5-year period (Lee and Barkstrom 1991, Lee *et al.* 1993). The measurements represent changes in the averaged differences between bolometric observations of space and of either the ICM activated shortwave lamp or blackbody. The measurement dropouts were caused by misalignment between the bolometers and the calibration sources. The misalignment occurred when the sensor scanning mechanism became sluggish (Kopia and Lee 1992). The ERBS flight calibration measurements demonstrate the maturity of the CERES ICM design. The ground ICM calibrations were used as quality checks on the design; and they did not yield radiometric references.

In Fig. 5, TRMM ICM and mirror attenuator mosaic (MAM) ground and flight calibration results are presented by Lee e*t al*. (1998), Priestley *et al.* (1998) and Priestley *et al.* (2000). Ground to on-orbit, the time series indicate that the total, shortwave, and window sensors responses maintained tied to the International Temperature Scale of 1990 at accuracy levels better than $\pm$ 0.2 $Wm^{-2}sr^{-1}$, $\pm$ 0.1 $Wm^{-2}sr^{-1}$, $\pm$ 0.3 $Wm^{-2}sr^{-1}$, respectively.

In Fig. 6, on-orbit, the January thruJune 2000 ICM results total and window sensor results indicate that the sensors' responses were stable at levels approaching $\pm$ 0.1 $Wm^{-2}sr^{-1}$. The ICM shortwave source, tungsten lamp, radiances drifted, increasing approximately 1 $Wm^{-2}sr^{-1}$. Therefore, the increasing trend in the shortwave sensor results does not indicate a drift in the shortwave sensor's response, but rather a drift in the calibration lamp's radiances. In the following paragraphs, solar calibration and validation results indicate that the shortwave sensor response was stable at the $\pm$ 0.3 $Wm^{-2}sr^{-1}$ level.

In Fig. 2 and at an elevation angle of 236 degrees, the second in-flight calibration system is called the mirror attenuator mosaic (MAM), a solar diffuser plate. The MAM is used to calibrate each the shortwave and total-wave channels using the solar radiances reflected from the MAM's. Each MAM consists of baffle-solar diffuser plate systems which guide incoming solar radiances into the instrument fields of view of the shortwave and total wave sensor units. The MAM baffle, solar view cover, and MAM are labeled in the Fig 1. The MAM diffuser plate consists of an array of

spherical aluminum mirror segments which are separated by a black paint reflecting surface. Thermistors are located in each MAM plate and in each MAM baffle. The CERES measurement precision goal was 1% (Folkman *et al.* 1993). The basic ERBE MAM calibration approach, flight data reduction algorithms, and in-flight performance yielded measurement precisions at the 3% level (Lee *et al.* 1992). In the following paragraph, the CERES basic solar calibration approaches are described.

The MAM calibration procedure includes measurements of the MAM before the Sun drifts into the MAM baffle field of view, of the MAM when the Sun is in the field of view, and after the Sun has drifted out of the view. During the MAM scan cycle of 6.6 seconds, the sensors make staring radiance measurements of first the MAM, second the ICM, and then cold space at the elevation angle of 169 degrees. The ICM is not activated during the MAM calibrations.

The total-wave and shortwave sensors are used to measure the MAM-reflected shortwave and longwave radiances as well as MAM emitted longwave radiances. For the shortwave sensor, the MAM-reflected shortwave radiances are equal to the differences between the MAM and cold space reference radiances. In the case of the total-wave sensor, the MAM radiances consist of both shortwave and longwave components. Therefore, for the total-wave sensor calibrations, the MAM-emitted and -reflected longwave radiances must be regressed against the MAM baffle and MAM structure temperatures in order to derive an empirical relation for the MAM longwave radiances as a function of MAM temperatures. The empirical relationship is used to define the longwave component of the mixed shortwave and longwave radiances from the MAM during flight calibrations.

The MAM is a relative calibration system. Its vectorial reflectances are not defined absolutely or spectrally. The ERBE MAM reflectances varied systematically with varying incidence angle as much as 20%. The CERES MAM is designed to reduce the reflectance variations. Laboratory and in-flight reflectance measurements of the CERES Proto-Flight Model MAM's indicate that systematic reflectance variations were reduced to less than $\pm$2.5%.

As shown in Fig. 6, the TRMM/CERES MAM solar calibration results indicate that the shortwave sensor response was stable at levels better than $\pm$ 0.3 Wm^{-2}sr^{-1} (Wilson *et al.* 1998). The total sensor response was found to be stable at the $\pm$ 0.5 Wm^{-2}sr^{-1} level.

Analyses of sensor offset stability are described in section 1.4.8 Zero-radiance offset determinations/calibration attitude maneuver (CAM).

1.4 POST-LAUNCH ACTIVITIES

 The TRMM/CERES sensors' flight gains and offsets were evaluated using in-flight calibrations and validation studies. The pre-flight laboratory-derived sensor gains and offsets (Lee *et al.* 1998) were used as the initial flight count conversion coefficients to convert the CERES sensor output signals into radiances. The time series of ground to early orbit ICM measurements as shown in Fig. 5, define the degree to which the sensors and ICM maintain the ground absolute calibrations, and if necessary the initial ground to flight corrections to the flight coefficients. In-flight ICM and

MAM calibrations, as shown in Fig. 6, are used to detect drifts or abrupt shifts in the sensors' responses and to determine revisions to the flight coefficients. Validation studies of the resulting CERES data products were used to verify sensor response changes or stabilities, indicated by in-flight calibrations. The CERES science team conducted detailed analyses of the first 8 months of in-flight calibrations and the validations to determine whether the sensor gains or offsets needed revisions. The flight coefficients (gains or offsets) are revised only if a sensor response changes by more than 0.5 $Wm^{-2}sr^{-1}$ in the longwave region or 0.8 $Wm^{-2}sr^{-1}$ in the shortwave region.

For the EOS Terra and Aqua missions, after six months of CERES data are collected, the validation tests in Section 1.3 will be applied. At that point we should be able to statistically determine mean differences between the historical ERBS radiances and CERES radiances to approximately 0.5 $Wm^{-2}sr^{-1}$ in longwave and 0.8 $Wm^{-2}sr^{-1}$ in shortwave. The validation plan requires 6 months of in-flight calibration results before any sensor count conversion coefficients can be revised. Thereafter, the empirical validation tests will be applied to each month of data separately in an attempt to determine if the gains and offsets are changing with time.

1.4.1 Planned Field Activities and Studies

N/A

1.4.2 New EOS-Targeted Coordinated Field Campaigns

N/A

1.4.3 Needs for Other Satellite Data

N/A

1.4.4 Measurements Needs (in situ) at Calibration/Validation Sites: Land, Buoys, etc.

The CERES are tied to international radiometric standards to a high accuracy by ground and on-board calibration systems. The addition of in situ measurements will not improve the accuracies of the instrument data products.

1.4.5 Needs for Instrument Development (Simulator)

The engineering model of the CERES instrument, normally used for ground based testing, was upgraded to the proto-flight model (PFM) instrument and launched on the TRMM spacecraft in order to maintain the TRMM launch schedule. The upgrading of the EM left the CERES program without a testbed instrument for the ground-based investigation of potential instrument anomalies. Therefore, CERES instrument simulators were built to test memory patches, and custom commands or instrument command sequences prior to uploading by telemetry link to the orbiting CERES instrument.

Instrument simulators serve as inexpensive devices to test customized instrument commands intended to solve in-flight anomalies of the instruments which could arise during the CERES

TRMM, EOS Terra, and Aqua Spacecraft missions. Each version (Chapman, 1998) of the CERES Instrument Simulator consists of electronic circuitry identical to the flight unit's twin microprocessors and telemetry interface to the supporting spacecraft electronics and two personal computers (PC) connected to the I/O ports that control azimuth and elevation gimbals. Flight simulation software consists of the unmodified TRW developed Flight Code and Ground Support Software specific to the platform under study which serves as the instrument monitor and also links NASA/TRW developed engineering models of the gimballed instrument. The CERES engineering development software models were modified to provide a virtual instrument running in real-time on a second PC linked to the flight microprocessors instrument control ports. The simulars lack only the radiometric outputs of the sensors. The first CERES Instrument Simulator duplicated the TRMM CERES instrument adequate enough to characterize the benchtop testing and functional verification of microprocessor loads for TRMM instrument uploads, down to the actual checksum.

Each simulator CPU consists of an 80C186 microprocessor on its own circuit card loaded with the TRW flight software stored in EPROM. Direct memory access (DMA) between the microprocessors and shared RAM for the telemetry linkage is used to communicate with the spacecraft or Bench Checkout Unit (BCU). The Ground Support Equipment (GSE) software running on the BCU dedicated PC serves as the instrument monitor. The BCU software was originally developed at TRW to provide a housekeeping screen of the telemetry parameters being monitored by the CERES instrument microprocessors while under test. Test instrument commands to be verified by the simulator are loaded into the GSE/BCU PC from the Command Maintenance Utility (CMU), then sent to the ICP via the telemetry link (which is accomplished by a coaxial cable for the simulator) to the Spacecraft Interface card. The GSE/BCU housekeeping screen displays the command status, the current and previous instrument mode, elevation and azimuth gimbal data, plus the microprocessor memory checksum data of the uploaded patch. Since the simulator has no real gimballed components, a second PC interfaced to the appropriate microprocessor control ports provides a separate virtual azimuth and elevation gimbal. Engineering software models of the elevation and azimuth gimbals have been modified to provide a fast, virtual instrument running in real time, interrupt linked to both the instrument control processing (ICP) and data asquisition processing (DAP) azimuth & elevation control ports.

 The TRMM version of the CERES Instrument Simulator had only one instrument to control whereas the Terra platform will have two instruments designated FORE (CEF) and AFT (CEA). Since the simulation system hardware is identical for both FORE and AFT either the CEF or CEA instrument specific code can be uploaded at any given time. Thus only one EOS AM-1 instrument simulation can be performed at a given time. The procedure is to upload the flight code specific to the desired instrument and conduct the simulation.

1.4.6 Geometric Registration Site/Geolocation

Geolocation is the process of locating a measurement in the Earth fixed coordinate system. The determination of the field of view (FOV) centroid location can be separated into two major steps. First, the unit pointing vector of the detector optical axis is calculated in the spacecraft local horizon system. Second, the detector pointing vector is transformed from the local horizon system into Earth fixed coordinates. Details of the CERES geolocation process are described by

Lee *et al* (1995) and Currey *et al.* (1998).

End-to-end validation and accuracy assessment techniques for the geolocation process require detection and geolocation of independent Earth features. For CERES, as with its predecessor ERBE, a technique for detecting coastlines under certain conditions and comparing their geolocated position with coastline maps was used (Hoffmann *et al,* 1987).

For ERBE the longwave channel displayed a characteristic signature when scanning high thermal contrast desert adjacent to ocean scenes. A typical coastline signature for the longwave channel is illustrated in Fig. 7. While the ocean maintains a relatively constant diurnal temperature, the desert temperature fluctuates resulting in a diurnal reversal in the slope of the coastline signature. A single longwave threshold value based on empirical data was used to filter out cloudy scenes. To reduce extraneous thermal contrast due to inland terrain, only data predicted to be within 25 km of the coastline was processed. Viewing angles were limited to 30 degrees from nadir to reduce the effect of atmospheric refraction. A cubic equation fit the signature well and the inflection point was assumed to represent the exact location of the coastline. The latitude and longitude of each inflection point was determined by interpolating between adjacent measurements. Coastline crossings for Baja, California [22 - 32 North latitude, 243-252 East longitude] are shown in Fig. 8. ERBE geolocation studies selected the coastlines of Australia [16-22 South latitude, 115-124 East longitude], Libya [30-33 North latitude, 14-23 east longitude], the Arabian Peninsula 16-24 North latitude, 52-61 East longitude], and Baja as validation targets. Latitude and longitude errors were determined for each scene by minimizing the least squares distance of the ensemble of crossings to the coastline map. These errors were transformed into cross track and along track errors for correlation with possible instrument error sources. Cross-track and along-track location errors were determined by averaging samples collected over extended time periods.

Hoffman *et al.* (1987) reported ERBS and NOAA-9 satellites passes from April 1985 had an average location error of less than 1.2 km, with the standard deviation of the error less than 5 km in both the along-track and cross-track directions. ERBE results with the coastline validation technique demonstrated that the technique was adequate for validating the geolocation process and evaluating long-term, end-to-end cross-track and along-track biases.

For CERES several improvements have been made to the coastline geolocation assessment process (Currey *et al* 1998). The current system allows unlimited coastline site selection. Validation targets are no longer limited to the four ERBE desert/ocean validation targets. Scenes with sharp longwave or visible gradients may be processed. Clear scenes are selected using the scene identification algorithm. Collection and processing of samples is fully automated. A time period is selected, clear coastal scenes extracted, and location errors are calculated for each scene. An additional interactive visualization system is available for quality and spot checks.

The CERES radiometer measurements are located at the "top of the atmosphere", 30 km above the WGS-84 ellipsoid model, and at the Earth's surface. The intersection of the instrument pointing vector with the Earth ellipsoid determines the measurement's surface geolocation. The surface geocentric latitude and longitude are defined in Earth fixed coordinates. Geocentric locations are converted to geodetic coordinates. The CERES surface geodetic locations are compared to the public domain World Bank II high resolution map which is digitized at

approximately 0.2 km resolution. A special version of the the World Bank II database, consisting of approximately six million vectors, was created with coastlines, islands, lakes, and rivers.

The coastline algorithm searches for coastlines by traversing a scanline and fitting four consecutive measurements to a cubic equation $y_i = ax_i^3 + bx_i^2 + cx_i + d$, where y_i is the radiance and x_i is the position of each measurement. The coefficients are solved by

$$\begin{bmatrix} a \\ b \\ c \\ d \end{bmatrix} = \begin{bmatrix} x_1^3 & x_1^2 & x_1 & 1 \\ x_2^3 & x_2^2 & x_2 & 1 \\ x_3^3 & x_3^2 & x_3 & 1 \\ x_4^3 & x_4^2 & x_4 & 1 \end{bmatrix}^{-1} \begin{bmatrix} y_1 \\ y_2 \\ y_3 \\ y_4 \end{bmatrix} \tag{11}$$

The inflection point, x = -b/3a, is considered a coastline crossing if it falls between x_2 and x_3, it is within a specified distance from the map, and a significant energy delta occurs between y_1 and y_4. Fig. 8 depicts a typical radiance scan as it crosses a coastline with an inflection point that meets the radiance threshold criteria. Separate night and day energy thresholds allow processing of both night and day scenes. Scenes must be cloud free to prevent false coastline detections. CERES scenes are screened for cloud contamination using the scene identification algorithm.

A minimization technique, the downhill simplex method, is used to minimize the average distance between the ensemble of crossings and the map database. The distance function is iteratively calculated by applying translational adjustments to each crossing location. The resultant shift in longitude and latitude is the location error for the scene. Since much of the location error may be attributed to the spacecraft attitude or the detector elevation assembly, errors are mapped into a coordinate system aligned with the spacecraft ground track and instrument scan axis.   The mapping of errors in geographic coordinates is shown in Fig. 9 and given by

$$\begin{bmatrix} \varepsilon_c \\ \varepsilon_a \end{bmatrix} = \begin{bmatrix} \mp\sin\eta & \mp\cos\eta \\ \cos\eta & \cos\eta \end{bmatrix} \begin{bmatrix} \varepsilon_\Lambda \\ \varepsilon_\phi \end{bmatrix} \tag{12}$$

where η is the spacecraft heading angle, ε_c is the cross-track error, ε_a is the along-track error, ε_Λ is the longitude error, and ε_ϕ is the latitude error. The along-track axis is positive in the direction of spacecraft flight. The cross-track axis is positive in the instrument scan direction. The upper sign (-) in Eq. (12) is used for left to right scans; the lower sign (+) is used for right to left scans. The coordinate systems, based on scan direction, support spacecraft +X axis and -X axis forward.

 Fig. 10 shows a TRMM coastline detection sample collected over South Africa on January 16,

1998. Spacecraft heading is -13.0° relative to the equator. The daytime radiance inflection threshold is 10 $Wm^{-2}sr^{-1}$ and the maximum viewing zenith is 30°. Detected crossings are drawn as circles. The minimization fitting technique calculates a longitude error of 0.0098° and a latitude error of 0.0052°. On the Earth's surface, this corresponds to an along-track error of 0.92 km and a cross-track error of -0.81 km. The location error for a single coastline scene may not be representative of the integrated instrument/satellite system. Additional satellite passes and different coastlines need to be investigated to identify systematic biases in the along-track cross-track coordinate system. Fig. 11 shows TRMM results for clear samples collected during January 1998. All samples were filtered for cloud contamination using corresponding VIRS scenes. The average cross-track bias is -0.58 km (σ = 1.11 km); the average along-track bias is 0.48 km (σ = 1.08 km).

Eight months of TRMM data has been run through the automated system. No significant changes occur in the monthly location errors. Average cross-track and along-track biases are -0.58 km and +0.48 km, respectively.

Since the CERES instrument performs a bidirectional scan there will be an opportunity to assess biases inherent in the technique due to scan direction, i.e. scanning from ocean to land vs. land to ocean. The instrument uses a biaxial scanning mode to acquire data for deriving angular direction models. Data obtained in the biaxial mode will scan a coastline from many different directions during a single pass. Data of this type may further enhance the potential for recovering biases due to scan direction or allow refinement of the cubic model used to define the detected coastline point.

1.4.7 Intercomparison Consistency (Multi-Instruments) Checks

1.4.7.1 - Single spacecraft - The single spacecraft sensor consistency checks involve intercomparisons of (1) the three sensors' filtered Earth radiance measurements in the same instrument package (TRMM and EOS platforms) and of (2) the filtered Earth radiance output signals from the same type of sensor in two difference instrument packages (EOS platform). Differences in the Earth radiance measurements will define the level of consistency. Angular distribution models (ADM) are used to account for the non-uniformity (anisotropy) of the target radiation fields.

The first intercomparison check was used in evaluating the consistency of the three Earth Radiation Budget Satellite scanning thermistor bolometer sensors. The evaluation approach is described in Section 1.3.3.3 and by Green and Avis (1996). For a particular geophysical scene like a desert, region of a ocean, land region, overcast cloud scene, etc., or the combination of all the scenes, the ratios of any two sensor outputs should be constant with time if the sensors' responses do not drift or shift. If changes in the ratios are observed, then, more detailed reviews of the calibration time series should be evaluated to determine the size and direction of possible response drifts or shifts in one or both of the ratioed sensors. In the consistency check, the ratios of sensor outputs will be monitored for all scenes. If changes in the ratios occur, then ratios will be collected and evaluated for different spectral scenes (overcast clouds, oceans, deserts, land, etc.) into to determine the spectral nature of the sensor changes.

In the second consistency check, on each EOS platforms, the stabilities of the same type of sensors can be evaluated. Operating both EOS instruments in the cross-track scan mode, many intercomparisons of the two shortwave, or total-wave, or window sensors Earth radiance measurements from the same geographical scene can be obtained. If both instruments are scanning in phase within $\pm$ 0.1 second, 2 pairs of intercomparison radiance measurements for each type of sensor and for every scan elevation position will be obtained every 6.6-second scan. Operating one instrument package in the cross-track scan mode and the other instrument in the rotating azimuth plane scan mode, 2 intercomparison radiance measurements from large (100 km) uniform scenes can be obtained at the nadir during a 6.6-second scan. At non-nadir elevation scan angles, the radiance intercomparions cannot be conducted at the radiance level because the emitted and reflected Earth radiation fields vary with the azimuth angle outside of the cross-track plane. For the non-nadir elevation angles, no intercomparisons will be conducted because angular distribution models (Green and Hinton, 1996) are required to account for the anisotropy of the target radiation fields and to convert the Earth radiances into unfiltered Earth irradiances.

1.4.7.2 - Multi-spacecraft - Using multi-spacecraft platform CERES instruments (TRMM and EOS AM-1, or TRMM and EOS PM-1, or EOS AM-1 and EOS PM-1), filtered radiance products will be compared for the same type of sensor (shortwave, or total-wave, or window) in order to determine the consistencies among data products from the different CERES instrument packages. At least four times a day, at the intersection point between the two spacecraft ground tracks, the sensors from both platforms should measure nadir Earth radiances from the intersection point within 30 minutes. In Fig. 12, the intersection point measurements from two different spacecraft platforms are illustrated. Two intersection points are night and the other two occur during the day. Since radiances are independent of the detector solid angle, then, the measurements from the two different platforms can be compared without correcting for the differences in attitude. No comparisons of radiance products at non-nadir scan elevation angles will be performed because angular distribution models are required to account for the anisotropy in the Earth emitted and reflected radiation fields.

 The EOS AM and PM platforms will have two identical CERES scanners that will be validated against each other (Section 1.4.7.1). In addition, each scanner will be used independently to establish the radiance statistics for earth validation targets. We will then us one as the standard and test for significant gain and offset changes between the two as in Section 1.3.3.1 and 1.3.3.2.

1.4.8 Zero-radiance Offset Determination/Calibration Attitude Maneuver (CAM)

In ground vacuum calibration facilities, CERES sensor offsets were found to vary with elevation scan angle position relative to the cold space measurement angle. In the case of longwave filtered radiance measurements, the variability can be as much as 0.6 $Wm^{-2}sr^{-1}$ or 0.8 $Wm^{-2}sr^{-1}$ for the shortwave measurements (Lee *et al.* 1998, Lee *et al.* 1999). As shown in Fig. 2, the space look angle position is located approximately 11 angular degrees below the spacecraft platform and above the Earth horizon. The observed offset variations can contribute as much as 1.3% to the uncertainty of the typical, Earth-reflected solar radiance scene of 63 $Wm^{-2}sr^{-1}$. Note that measurement uncertainties of the order of 0.25 $Wm^{-2}sr^{-1}$ are required to detect long-term climate changes. Therefore, to reach the 0.25 $Wm^{-2}sr^{-1}$ uncertainty level, the sensor offset variability with scan angle must be accounted for in the processing of the filtered radiances.

The offset variations with scan angle are caused by gravitational effects, and by electro-magnetic induced (EMI) electronic noise. In ground vacuum calibration facilities, the offset variations due to gravity were minimized using a measurement geometry in which the elevation plane of the scan angles was oriented perpendicular to the gravity vector. The offset variations were determined with the plane of the scan angular measurements oriented perpendicular (minimum gravity effects) and parallel (maximum gravity effects) to the gravity vector. The TRMM and EOS AM-1 sensor offset variations with the alignment of the gravity vector were analyzed to produce a model which characterize the impact of gravity upon the offsets. The analyses failed to produce an adequate model. Therefore, on-orbit observations of cold space are required to characterize adequately the offset variability with elevation scan angle and scanning configuration.

In Figs. 13, 14, and 15, for the minimum gravity effects geometry, ground-derived TRMM and EOS AM-1 CERES offset variations are presented as a function of scan position in digital counts. For the shortwave and window sensors, 10 counts are equal to 1 $Wm^{-2}sr^{-1}$ while, for the total sensor, approximately 7 counts are equal to 1 $Wm^{-2}sr^{-1}$.

In Fig. 13, the pre-launch TRMM/proto-flight model (PFM) offsets are presented as functions of the scan sample number position and scan elevation angle. During July 1995, the PFM offsets were measured in the TRW 137-cm diameter vacuum facility, operated at 10^{-5} torr. The sensor's output voltage was sampled every 10 ms during the 6.6-second scan cycle. The scan sample position indicates the chronological order in which the output voltage was sampled and digitized. There are 660 scan samples. The solid line defines the relation between sample number position and sensor elevation angle. For the TRMM orbit, positions 1 through 39 correspond to the radiance measurements of cold space at an elevation angle of 10.558 degrees. Positions 40 through 290 correspond to Earth radiance measurements, scanning from an elevation angle of 10.558 near one limb of the Earth, across the Earth to the other limb near the angle of 169.442. Positions 291 to 311 correspond to observations of cold-space radiances on the other side of the Earth at the elevation angle of 169.442 degrees. Positions between 320 and 340 correspond to observations of built-in, internal calibration module (ICM) sources (tungsten lamp and in-flight blackbodies) at the angle of 194.002 degrees. On the scan retrace, sample positions 349 through 369 correspond to space radiance measurements at 169.442 degrees; 370 to 621 correspond to Earth radiance measurements, scanning back across the Earth; and 621 to 660 correspond to space radiances at the elevation angle of 10.558 degrees.

In Fig. 13, for the positions corresponding to Earth radiance measurements, the pre-launch TRMM PFM sensor offset data indicated that the shortwave and window sensor offsets varied as much as 1.5 digital counts from the cold space offsets. For the total sensor, the variations were found to be less than 0.5 count. The total sensor output voltage should be approximately 450 counts for the globally-averaged earth longwave radiance of 76 $Wm^{-2}sr^{-1}$. The window sensor voltage should be approximately 110 counts for the same longwave radiance level. The shortwave sensor voltage should be approximately 400 counts for the globally-averaged shortwave radiance of 63 $Wm^{-2}sr^{-1}$. Therefore, the shortwave sensors' offset variations can affect resulting radiance calculations as much as 0.4%.

In Figs. 14 and 15, the EOS AM-1, flight model one (FM1) and flight model two (FM2) zero-radiance offsets are presented as functions of scan elevation angle and sample number position. The offsets were measured in the TRW Radiometric Calibration Facility (RCF) in a vacuum environment of 10^{-5} torr. Note that the normal sensor elevation angle scan profile for the EOS AM-

1sensors is different from that of the TRMM sensors. For example, the cold-space measurements occur at an elevation angle of 18 degrees, instead of TRMM 10.6 degrees. For the FM1 and FM2 sensors, the offsets, corresponding to the Earth radiance measurements at sample number positions 40-290 and 370-621, were found to be less than 1 digital count below the space offsets. The FM1 shortwave sensor offset variations were greater than those for total and window sensors. For the FM2 shortwave and window sensors, the offsets, corresponding to the Earth radiance measurements varied as much as 1.5 digital counts from the space offsets. The FM2 total sensor exhibited variations less than 0.5 count. From the offset determinations, the typical sensor noise equivalent-radiance (NER) was found to be approximately 1 digital count ($0.1 \ Wm^{-2}sr^{-1}$).

During spacecraft calibration attitude maneuvers (CAM), on-orbit CERES sensor offsets were determined from measurements of the zero-radiances of cold space as a function of scan elevation angle. It should be noted that the moon represents a significant broadband target of approximately $20 \ Wm^{-2}sr^{-1}$ for the CERES total sensor. During the CAM's, the TRMM spacecraft was held in an inertially-fixed configuration in which the spacecraft nadir was pointed away from the Sun in the direction of deep space. In Fig. 16, the TRMM CAM geometry is illustrated.

January 7-8, 1998, six separate non-consecutive TRMM CAM orbits were performed. During CAM orbit number 1, offsets were determined in the cross-track (scan plane oriented perpendicular to the orbital plane) and in the biaxial (scan plane rotated at a constant rate of 6 degrees per second relative to the orbital plane) modes. During CAM orbits numbers 2 and 4, offset measurements were conducted in the cross-track mode only. CAM orbits 3 and 5 were dedicated to offset determinations in the biaxial mode, while CAM orbit number 6 was dedicated to measurements in the biaxial short scan mode, and in the along-track scan mode, in which the plane of the scan elevation angles was located in the orbital plane.

The analyses of the TRMM CAM on-orbit measurements indicated that the sensors' offsets varied with elevation angle and that the offsets were not affected by sensor scan plane rotation or its orientation with respect to the orbital plane. Analyses of TRMM CAM orbits 2 and 4 indicated that the total, shortwave, and window sensors' earth-viewing offsets were typically 1.5 counts lower than the sensor offsets corresponding to the cold-space offsets, obtained at the elevation angle of 10.558 degrees.

In Fig. 17, for the cross-track scan configuration, the on-orbit, TRMM total sensor offset variations were found to be 0.4 to 1 count lower than the corresponding pre-launch offsets, presented in Fig. 9. In Fig. 13, offset variations, corresponding to the cross-track scan configuration, were found to be in excellent agreement with those from the RAP normal and short scan configurations. The along-track offset variations were found to be 0.6 count lower than those for the cross-track and Rap configurations. For all scan configurations, the one sigma standard deviations were found to be approximately 0.6 count. These results are confusing since the along-track variations suggest some dependence upon azimuth angle whereas the RAP variations do not show a dependence on azimuth angle.

In Fig. 18 for the cross-track scan configuration, the on-orbit shortwave sensor offset variations were found to be approximately 0.2 to 0.4 count higher than the corresponding pre-launch, ground-derived offset variations, illustrated in Fig. 13. In Fig. 17, the on-orbit offset variations, corresponding to the cross-track scan configuration, were found to be approximately 0.6 count higher than those corresponding to the along-track, and biaxial/RAP scan configurations. For the cross-track and along-track configurations, the one sigma standard deviations from the means were 1.0 count. However, for the RAP normal and short configurations, the standard deviations

were found to be higher at the 1.6 counts levels. The above results suggest that the offset varia-
tions suggest some dependence upon azimuth angle.

In Fig. 19, for the cross-track configuration, the on-orbit, TRMM window sensor offset variations
were found to be 0.2 to 0.4 count higher than the pre-launch ones. The cross-track variations were
found to be approximately 0.2 count higher than those for the RAP and along-track configura-
tions. The standard deviations were found to be 0.8 count for all three scan configurations. These
results indicate very a weaker dependence upon azimuth angle.

The discussed TRMM, on-orbit results indicate that ground-derived offsets may not be adequate
enough to characterize the on-orbit offset variations with elevation scan angle.

Within 100 days after the EOS AM-1 Spacecraft launch, CAM's will be performed to determine
the variations in CERES sensor offsets with scan angle. Each EOS AM-1 CAM will be approxi-
mately 33 minutes in duration. CERES has requested six separate CAM orbits.

In Figs. 20 and 21, the CAM geometry is illustrated in which the spacecraft will be pitched at an
inertial rate of 0.122 angular degrees per second. For the CERES instrument, the Earth will be
partially obstructing the sensors' fields-of-view during the first 13 and the last 13 minutes of the
each CAM. Therefore, during a single CAM, only 7 minutes of unobstructed cold space observa-
tional time will be available to define the variations of the sensors' zero-radiance offsets scan
angle or geometry. The unobstructed observations will provide approximately

CERES has requested six, non-consecutive CAM orbits, similar to the number of CAM which
were provided during the TRMM Spacecraft program during January 7-8, 1998, and which were
described in the previous paragraphs. During the first CAM, offset variations will be measured in
the cross-track, RAP/biaxial normal, RAP/biaxial short, and along-track scan configurations. Dur-
ing the second and third CAM's, the offset variation measurements biaxial will be conducted in
the normal and biaxial short configurations, respectively. The fourth and fifth CAM's should be
conducted in the along-track and cross-track configurations, respectively. The sixth CAM should
be conducted in all four configurations, similar to the first CAM.

Radiometric measurements of the nighttime side of the Earth can be used to validate the on-orbit
CERES determinations of offset variation with scan angle. The nighttime Earth shortwave radi-
ance should be zero by definition. The CERES shortwave sensors are sensitive to longwave radi-
ances in the 0.3 - 5.0 µm, and in the >60 µm spectral regions.

There are no known engineering risks associated with CAM's. The CERES LaRC Project and
Science Team have considerable experience in applying CAM deep space radiometric
measurements in the level 1 data processing algorithms.

1.5 IMPLEMENTATION OF VALIDATION RESULTS IN DATA PRODUCTION

1.5.1 Approach (Include Long-Term Calibration considerations)

   The most important problem with implementing the empirical validation results as outlined in
this section is to decide on the absolute standard. Most of the discussion here has been on validat-
ing one set of data against another. The purpose of ground based and in-flight calibration is to tie
the satellite measured radiances to an international standard. However, from experience we know

that instruments change in space and that in-flight calibration methods have their own set of problems. Thus, when two sets of satellite data show statistically significant differences, how do we decide which is correct or best? The answer will lie in examining all validation test from the various systems and searching for adjustments (be they zero) that give the most consistency and best explain the observations.

Although the validation tests in this section say little about accuracy to an international standard, they say much about precision and long-term stability. Using earth validation targets, we would expect to detect instrument drift changes in the order of 0.1% (Green and Avis 1996).

1.5.2 Role of EOSDIS

Operational EOSDIS level 1 radiance data products will be used as source data for the validation studies, performed off-line, using science computing facilities (SCF).

1.5.3 Plans for Archival of Validation Data

The CERES in-flight calibration systems data will be stored in the world-wide web home pages and in the CERES science computing facilities. Results and summaries of the in-flight calibration and geolocation studies will be forwarded for publication in referenceable reports.

1.6 SUMMARY

This geolocation and calibrate validation plan is designed to verify the accuracies of the CERES filtered shortwave and longwave radiances; and the geographicaly locations of the target scenes. Each CERES instrument consists of broadband total (0.3 μm - >100μm), shortwave (0.3 μm - 5.0 μm), and narrowband water vapor (8 μm - 12 μm) spectral thermistor bolometer sensors. November 27, 1997, the first set [proto-flight model] of CERES sensors was launched aboard the Tropical Rainfall Measuring Mission (TRMM). On December 27, 1997, the sensors produced its first measurements of the Earth-reflected solar (0.3 μm - 5.0 μm) and Earth-emitted longwave (5 μm - >100 μm) filtered radiances. In, 1999, the second [flight model 1] and third [flight model two] sets of CERES sensors are scheduled for launch on the Earth Observing System (EOS) Terra Spacecraft. Mid-1999, the fourth [flight model 3] and fifth [flight model 4] were delivered for intergration into the EOS Aqua Spacecraft. EOS PM-1 is scheduled for launch in December 2000.

Using the TRMM/CERES in-flight calibration systems and thermistor bolometer sensors, the CERES Science Team demonstrated the successful transfer of the ITS-90 temperature-based absolute radiometric scale from the ground calibration facilities into orbit at uncertainty levels approaching $\pm$ 0.1 $Wm^{-2}sr^{-1}$. In addition, the geolocation calculations of CERES radiance measurement footprints were validated at the $\pm$ 0.5 km uncerainty level. The calculations were derived from information on the ground alignment knowledges of the CERES sensors relative to the instrument axes, and of the spacecraft coordinate system axes as well as upon the ephemeris of the spacecraft. The sensor pointing knowledge was determined from inflective changes in the sensors' responses as measured radiances from coastlines where high thermal contrasts existed between deserts and oceans.

1.7 REFERENCES

Avis, L. M., J. Paden, R. B. Lee III, D. K. Pandey, J. C. Stassi, R. S. Wilson, C. J. Tolson, and W. C. Bolden, 1994: NOAA-9 Earth Radiation Budget Experiment (ERBE) scanner offsets determination, *NASA Technical Memorandum* **109086** (NASA Langley Research Center, Hampton, VA 23681-0001), 26 pages.

Barkstrom, B. R., 1984: The Earth radiation budget experiment (ERBE), *Bull. Am. Meteorol. Soc.,* **65**, 1170-1185.

Barkstrom, B. R., and G. L. Smith, 1986: The Earth radiation budget experiment: Science and

Bush, K. A., G. L. Smith, D. A. Rutan, B. R. Barkstrom, R. B. Lee III, and D. F. Young, 1999: The Earth Radiation Budget Satellite 13-year data set, Presented at *Third Symposium on Integrated Observing Systems* [sponsored by American Meteorological Society), January 10-15, 1999, Dallas, Texas.

Folkman, M. A., P. J. Jarecke, L. A. Darnton, T. D. Hedman, and R. B. Lee III, 1993: Design of a solar diffuser for on-orbit calibration of the Clouds and the Earth's Radiant Energy System (CERES) instruments, *Proc. of SPIE*, **1939**, 72-81.

Currey, Chris, Lou Smith, and Bob Neely, 1998: Evaluation of Clouds and the Earth's Radiant Energy System (CERES) scanner pointing accuracy using coastline detection system, *Proc. of SPIE*, **3439**, 367-376.

Currey, Chris, R. N. Green, 1999:Validation of the CERES shortwave measurements over desert and cloud scenes, *10th Conference on Atmospheric Radiation*, American Meteorological Society, 567-570.

Chapman, John J., 1998: A Benchtop Instrument Simulator for CERES/EOS-AM1, *Proc. of SPIE*, **3439**, 355-366.

Green, R. N. and L. M. Avis, 1996: Validation of ERBS Scanner Radiances, *J. Atmos. Ocean Technol.*, **13**, 851-862.

Green, R. N., and R. O. Hinton, 1996: Estimation of angular distribution models from radiance pairs, *J. Geophys. Res.*, 101, 16951-16959.

Halyo, N., D. K. Pandey, and D. B. Taylor, 1989: Modeling and characterizations of the Earth Radiation Budget Experiment (ERBE) nonscanner and scanner sensors, *NASA Contractor Report* **181818**.

Hoffmann, L. H., W. L. Weaver, and J. F. Kibler, 1987: Calculation and accuracy of ERBE scanner measurement locations, *NASA Technical Paper* **2670**, NASA Langley Research Center, Hampton, Va. 23681-0001.

Jarecke, P. J., M. A. Folkman, and L. A. Darnton, 1991: Radiometric calibration plan for the Clouds and the Earth's Radiant Energy System instruments, *Proc. of SPIE*, **1493**, 244-254.

Jarecke, P. J., M. A. Folkman, T. R. Hedman, and M. E. Frink, 1993: Clouds and the Earth's Radiant Energy System (CERES): Long-wave calibration plan and radiometric test model (RTM) calibration results, *Metrologia*, **30**, 223 -230.

Kopia, L. P. and R. B. Lee III, 1992: Thermistor Bolometer Scanning Radiometer-Applications and Flight Experience, *Optical Engineering*, **31**, 156-165.

Kratz, D. P., and F. G. Rose, 1999: Accounting for molecular absorption within the spectral range of the CERES window channel, *J. Quant. Spectrosc. Radiat. Transfer*, Vol. 61, No. 1, pp. 83 -95.

Kratz, D. P., K. J. Priestley, and R. N. Green, 2000: Establishing the relationshjip between the CERES total and window channel measured radiances for conditions involving deep convective clouds, *J. Geophys. Res.* (submitted).

Lee, R. B.,III, B. R. Barkstrom, N. Halyo, M. A. Gibson, and L. M. Avis, 1989: Characterizations of the Earth Radiation Budget Experiment (ERBE) scanning radiometers, *Proc. of SPIE*, **1109**, 186-194.

Lee, R. B., III, and B. R. Barkstrom, 1991: Characterization of the Earth Radiation Budget Experiment Radiometers, *Metrologia*, **28**, 183-187.

Lee, R. B., III,L. M. Avis, M. A. Gibson, and L. P. Kopia, 1992: Characterizations of the mirror attenuator mosaic: solar diffuser plate, *Applied Optics*, **31**, 6643-6652.

Lee, R. B., III, L. M. Avis, M. A. Gibson, S. Thomas, and R. Wilson, 1993: In-flight evaluation of tungsten lamps using shortwave thermistor bolometers and active-cavity radiometers, *Metrologia*, **30**, 389-395.

Lee, R. B., III, B. A. Childers, G. L. Smith, J. Paden, D. K. Pandey, and S. Thomas, 1996a: Clouds and the Earth's Radiant Energy System (CERES) instrument level 1 science data validation plan for geolocated radiances, *Proc. of SPIE*, **2820**, 105-116.

Lee, R. B., III, B. R. Barkstrom, G. L. Smith, J. E. Cooper, L. P. Kopia, R. W. Lawrence, S. Thomas, D. K. Pandey, M. A. Gibson, and D. A. H. Crommelynck, 1996b: The Clouds and the Earth's Radiant Energy System (CERES) Sensor and Pre-Flight Calibration Plans, J. Atmos.and Ocean Technol.,**13**, 300-313.

Lee, R. B., III, G. L. Smith, B. R. Barkstrom, K. J. Priestley, S. Thomas, J. Paden, D. K. Pandey, W. C. Bolden, and R. S. Wilson, 1997: Pre-launch calibrations of the Clouds and the Earth's Radiant Energy System (CERES) Tropical Rainfall Measuring Mission and Earth Observing System (EOS) Morning (AM-1) Spacecraft thermistor bolometers, *Proc. of SPIE*, **3117-37**, 281-293.

Lee, Robert B., III, B. R. Barkstrom, Herbert Bitting, Dominique A. H. Crommelynck, J. Paden, D. K. Pandey, K. J. Priestley, G. L. Smith, S. Thomas, K. L. Thornhill, and R. S. Wilson, 1998: Pre-Launch Calibrations of the CERES Tropical Rainfall Measuring Mission (TRMM) and Earth Observing System (EOS) Morning (AM)-1 Spacecraft Thermistor Bolometers, *IEEE: Transactions* on Geoscience and Remote Sensing, **36**, 1173-1185.

Lee, R. B. Lee III, S. Thomas, B. R. Barkstrom, J. Paden, D. K. Pandey, K. J. Priestley, G. L. Smith, A. Y. Al-hajjah, and R. S. Wilson, 1999: Analyses of on-orbit determinations of the Clouds and the Earth's Radiant Energy System (CERES) thermistor bolometer sensor zero-radiance offsets, *Proc. of SPIE*, **3333** , Presented at July 18-23 1999 Spie Annual Meeting, Denver, CO.

Loeb, N. G., K. J. Priestley, D. P. Kratz, E. B. Geier, R. N. Green, B. A. Wielicki, P. O. Hinton, and S. K. Nolan, 2000: Determination of the Unfiltered Radiances from the Clouds and the Earth's Radiant Energy System (CERES) Instrument, *J. of Appl. Meteor.* (Accepted)

Paden, J.; G. Louis Smith, R. B. Lee, III, D. K. Pandey, K. J. Priestley, G. L. Smith, S. Thomas, K. L. Thornhill, and R. S. Wilson, 1998: Comparisons between Point Response Function measurements and theory for the Clouds and the Earth's Radiant Energy System (CERES) TRMM and the EOS-AM spacecraft thermistor bolometer sensors, *Proc. of SPIE*, **3439**, 344-354.

Pandey, D. K., R. B. Lee III, J. Paden, S. thomas, K. L. Thornhill, R. S. Wilson, K. J. Priestley, B. R. Barkstrom, G. L. Smith, and H. Bitting, 1998: Cryogenically Cooled Transfer Active Cavity Radiometer (TACR) for Radiometric Characterizations of the Clouds and the Earth's Radiant Energy System (CERES) scanning thermistor bolometers, *Proc. of SPIE*, **3439**, 335-343.

Press, W., B. Flannery, S. Teukolsky, and W. Vetterling, *Numerical Recipes in C*, pp. 305-309, Cambridge University Press, Cambridge, 1988.

Priestley, K. J., L. P. Kopia, R. B. Lee, III, J. R. Mahan, Haefflin, G. L. Smith, and J. Paden, 1997: Use of First-Principal Numerical Models to Enhance the Understanding of the CERES Point Spread Function.*Proc. SPIE*, **3221**, pp. 191.

Priestley, K. J, R. B. Lee,, III, B. R. Barkstrom, S. Thomas, K. L. Thornhill, J. Paden, D. K. Pandey, R. S. Wilson, H. C. Bitting, and G. L. Smith, 1998: Radiometric stability of the Clouds and the Earth's Radiant Energy System scanning thermistor bolometers, *Proc. of SPIE*, **3439**, 303-314.

Priestley, K. J., B. R. Barkstrom, R. B. Lee, R. N. Green, S. Thomas, R. S. Wilson, P. L. Spence, J. Paden, D. K. Pandey, and A. Al-hajjah, 2000: Post launch radiometric validation of the Clouds and the Earth's Radiant Energy System (CERES) proto-flight model on the Tropical Rainfall Measuring Mission (TRMM) Spacecraft through 1999, *J. of Appl. Meteor.* (In Press)

Rutan, D. A., G. L. Smith, T. P. Charlock, and R. N. Green, 1999: Early intercomparisons of CERES and ERBE results, Presented at *Third Symposium on Integrated Observing Systems* [sponsored by American Meteorological Society), January 10-15, 1999, Dallas, Texas.

Smith, G. L., R. B. Lee, III, B. R. Barkstrom, Bruce A. Wielicki, K. J. Priestley, S. Thomas, J. Paden, R. S. Wilson, D. K. Pandey, K. L. Thornhill, 1998: Overview of CERES Sensors and In-flight Performance, *Proc. of SPIE*, **3439**, 292-302.

Smith, G. L., D. K. Pandey, A. Al-hajjah, B. R. Barkstrom, R. B. lee, J. paden, K. J. Priestley, S. Thomas, and R. S. Wilson, 2000: Determination and validation of slow-mode properties of the Clouds and the Earth's Radiant Energy System (CERES) scanning thermistor bolometers, *Proc. of SPIE*,4135, (In Press).

Staylor, W. F., 1986: Site selection and directional models of deserts used for ERBE validation targets, NASA Technical Paper 2540.

Staylor, W. F., 1993: Stability of the Earth Radiation Budget Experiment scanner results for the first two years of multiple-satellite operation, *J. Atmos. and Ocean Tech.*, **10**, 827-832.

Thomas, S., B. R. Barkstrom, R. B. Lee III, K. J. Priestley, H. Bitting, J. Paden, D. K. Pandey, G. L. Smith, K. J. Thornhill, and R. S. Wilson, 1998: Flight and ground calibrations: TRMM and EOS-AM1 Clouds and the Radiant Energy System (CERES) Instrument zero radiance offsets determinations, *Proc. of SPIE*, **3439**, 315-324.

Thornhill, K. L., H. Bitting, R. B. Lee,III, J. Paden, D. K. Pandey, K. J. Priestley, S. Thomas, and R. S. Wilson, 1998: Spectral Characterizations of the Clouds and the Earth's Radiant Energy System (CERES) Thermistor Bolometers Using Fourier Transform Spectrometer (FTS) Techniques, *Proc. of SPIE*, **3361**, 55-65.

Turner, M. S., 1993: Why is the temperature of the universe 2.726?, *Science*, **262,** 861-867.

Wielicki, B. A. and B. R. Barkstrom, 1991: Clouds and the Earth's Radiant Energy System (CERES) - An Earth Observing System Experiment. *Second Symposium on Global Change Studies* - Preprints Am. Meteorol. Soc., 11-16.

Wielicki, B. A., B. R. Barkstrom, E. F. Harrison, R. B. Lee III, G. L. Smith, and J. E. Cooper, 1996: Clouds and the Earth's Radiant Energy System (CERES): An Earth Observing System Experiment, *Bull. American Meteorological Soc.*, **77**, 853-868.

Wielicki, B. A.; Barkstrom, B. R.; Baum, B. A.; Charlock, T. P.; Green, R. N.; Kratz, D. P.; Lee, R. B.; Minnis, P.; Smith, G. L.; Wong, T.; Young, D. F.; and the CERES Science Team, 1998: Clouds and the Earth's Radiant Energy System (CERES): Algorithm Overview. *IEEE: Transactions* on Geoscience and Remote Sensing, **36**, 1127-1141.

Wilson, R. S.; R. B. Lee, B. R. Barkstrom, H. Bitting, D. K. Pandey, K. J. Priestley, G. L. Smith, S. Thomas, and K. L. Thornhill, 1998: On-Orbit solar calibrations using the TRMM Clouds and the Earth's Radiant Energy System (CERES) in-flight calibration system, *Proc. of SPIE*, **3439**, 325-334.

Table 1   CERES Instrument Accuracy Requirements (1 Sigma)

Detector	Shortwave		Total		Window
Spectral Region	$0.3 \rightarrow < 5.0 \, \mu m$		$0.3 \rightarrow > 100 \, \mu m$		$8 \rightarrow 12 \, \mu m$
Scene Levels	Less < 100 $Wm^{-2}sr^{-1}$	Greater > 100 $Wm^{-2}sr^{-1}$	Less < 100 $Wm^{-2}sr^{-1}$	Greater > 100 $Wm^{-2}sr^{-1}$	All Levels
Accuracy Requirements	0.8 $Wm^{-2}sr^{-1}$	1.0%	0.6 $Wm^{-2}sr^{-1}$	0.5%	0.3 $Wm^{-2}sr^{-1}$
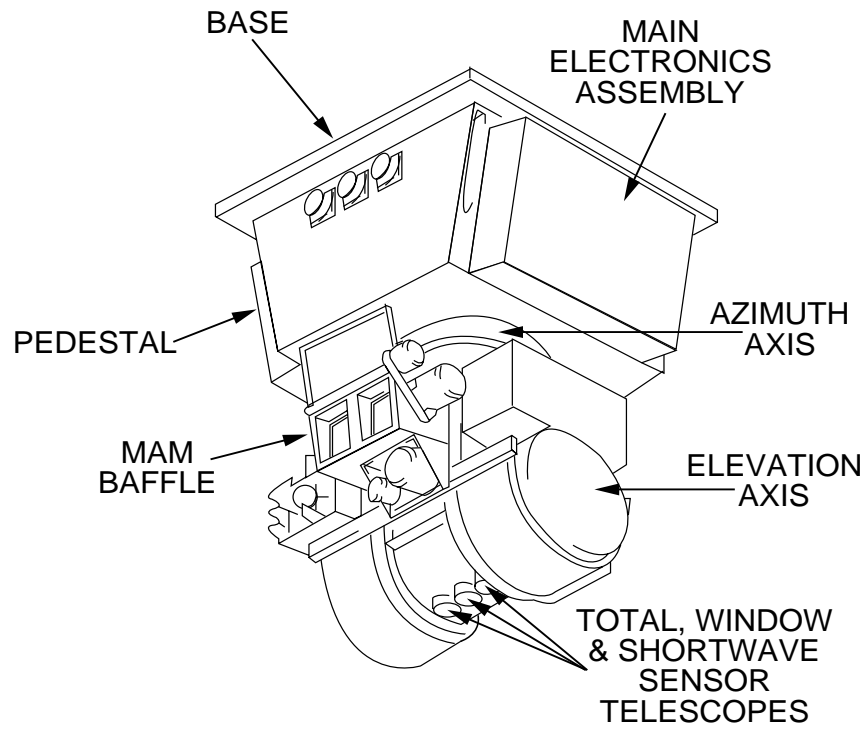
Fig. 1. CERES scanning sensor package
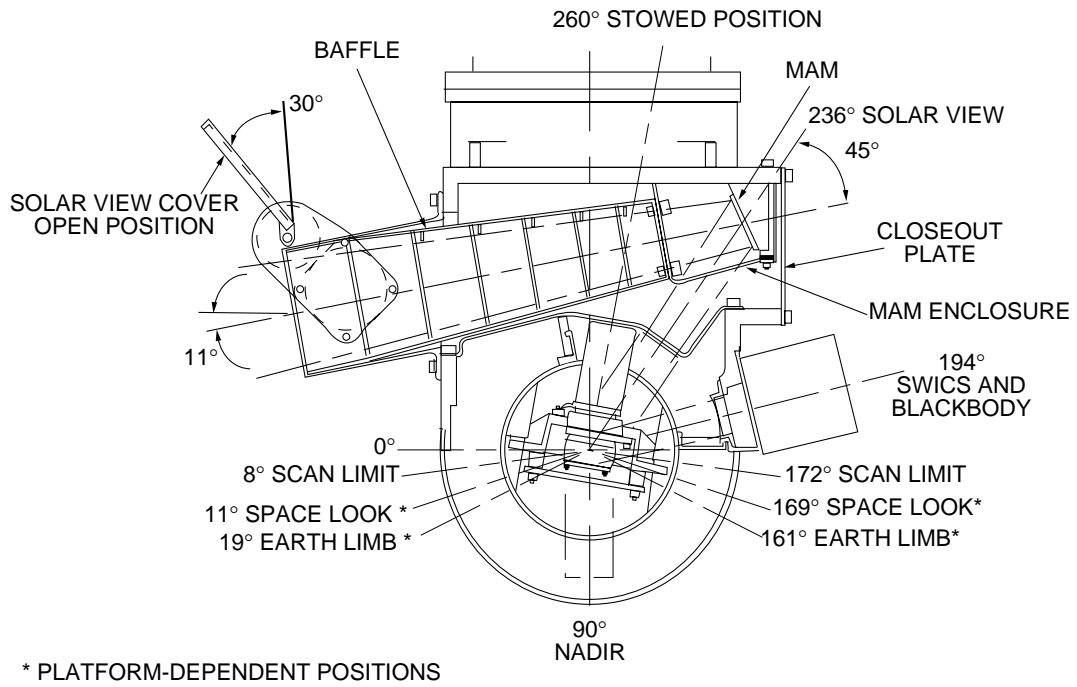
Fig. 2. TRMM Spacecraft, CERES sensors elevation plane scanning geometry and flight calibration.

.
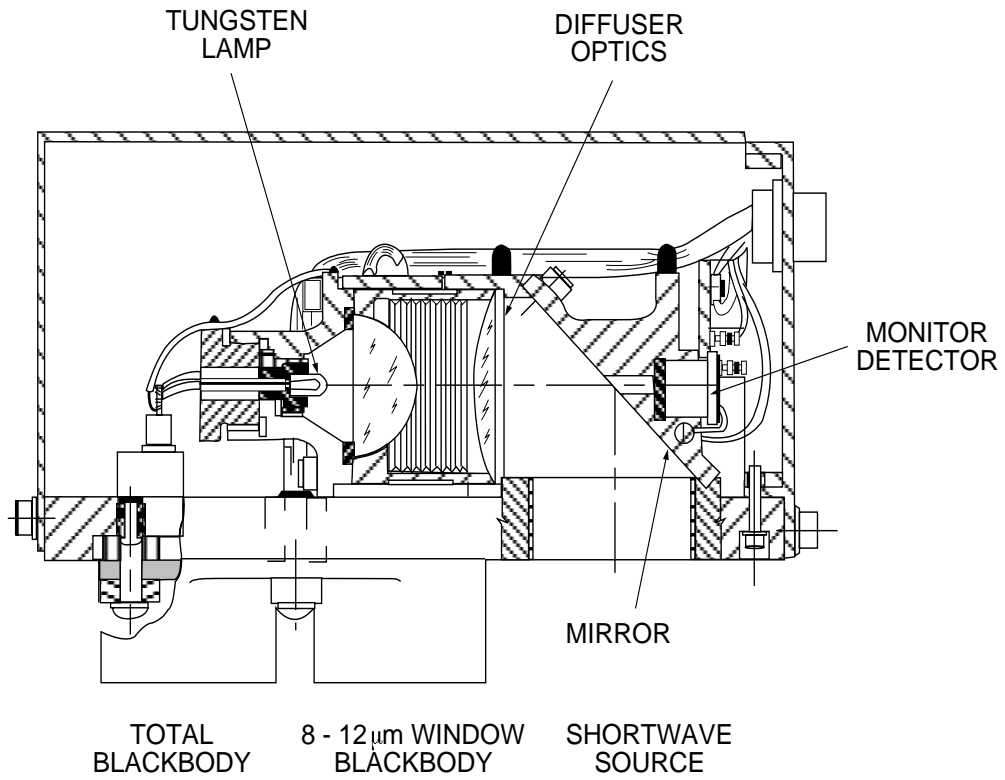
Fig. 3. Schematic diagram of CERES Internal calibration module(ICM)
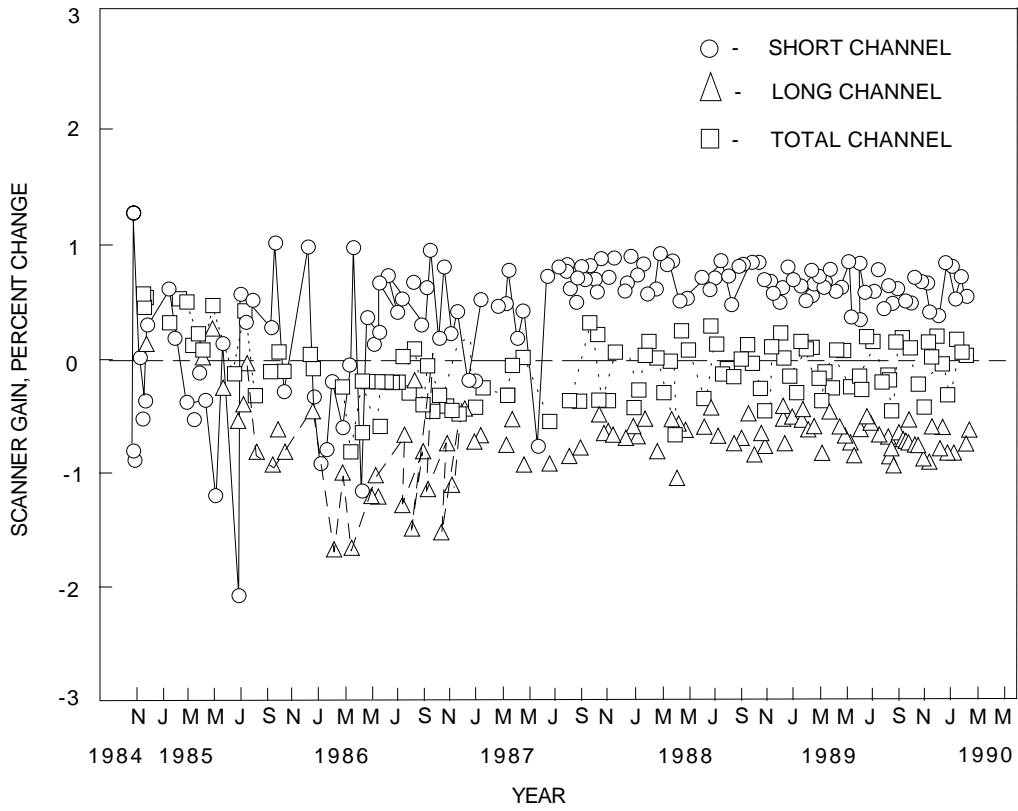
Fig. 4. ERBS thermistor bolometer flight calibration using the internal calibration module (ICM).

**CERES TRMM/PFM SENSOR CALIBRATIONS
USING CONSTANT LEVEL 3
(NORMALIZED TO JAN. 4, 1998 VALUES)**
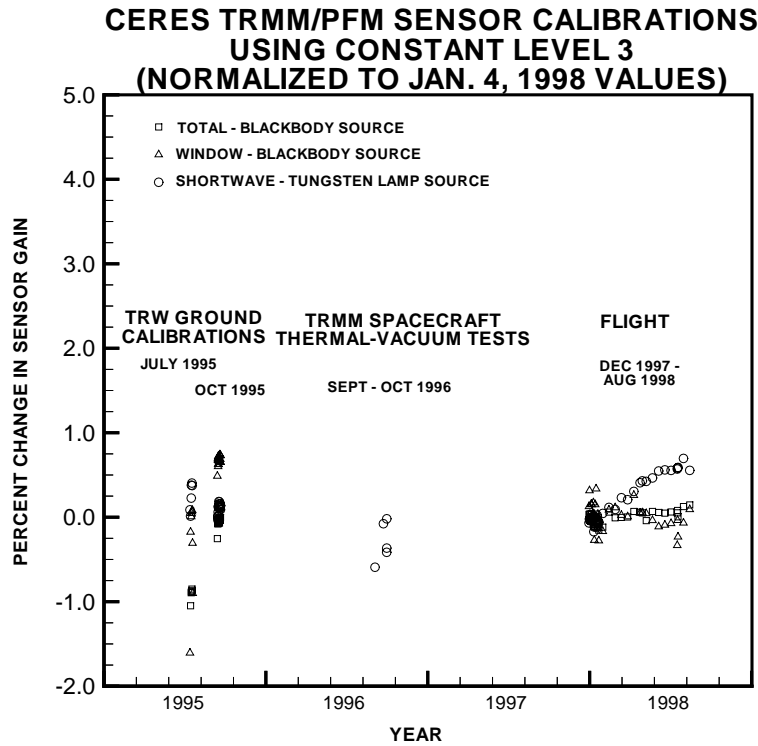
Fig. 5. Ground and on-orbit CERES internal calibration module (ICM) measurements of sensor response/gain changes are presented for the August 1995 thru August 1998 period.
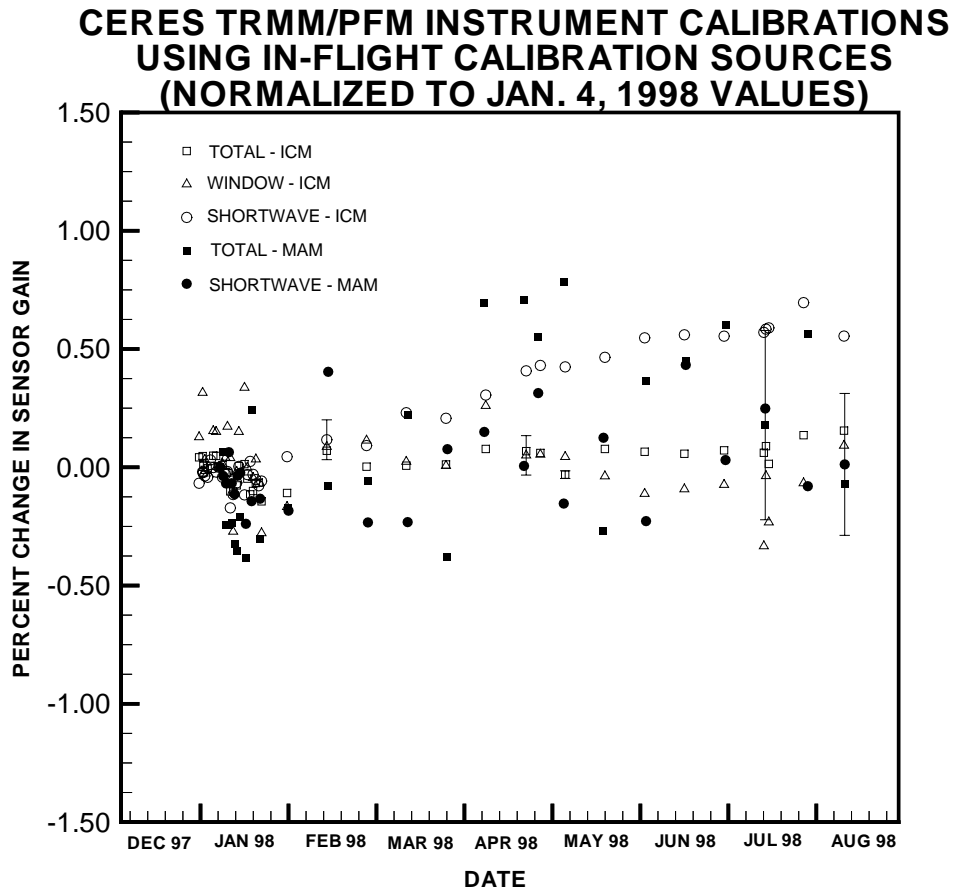
Fig. 6. On-orbit CERES internal calibration module (ICM) and mirror attenuator mosaic (MAM) sensor gain changes measurements are presented for the December 27, 1998 thru August 31, 1998 period.
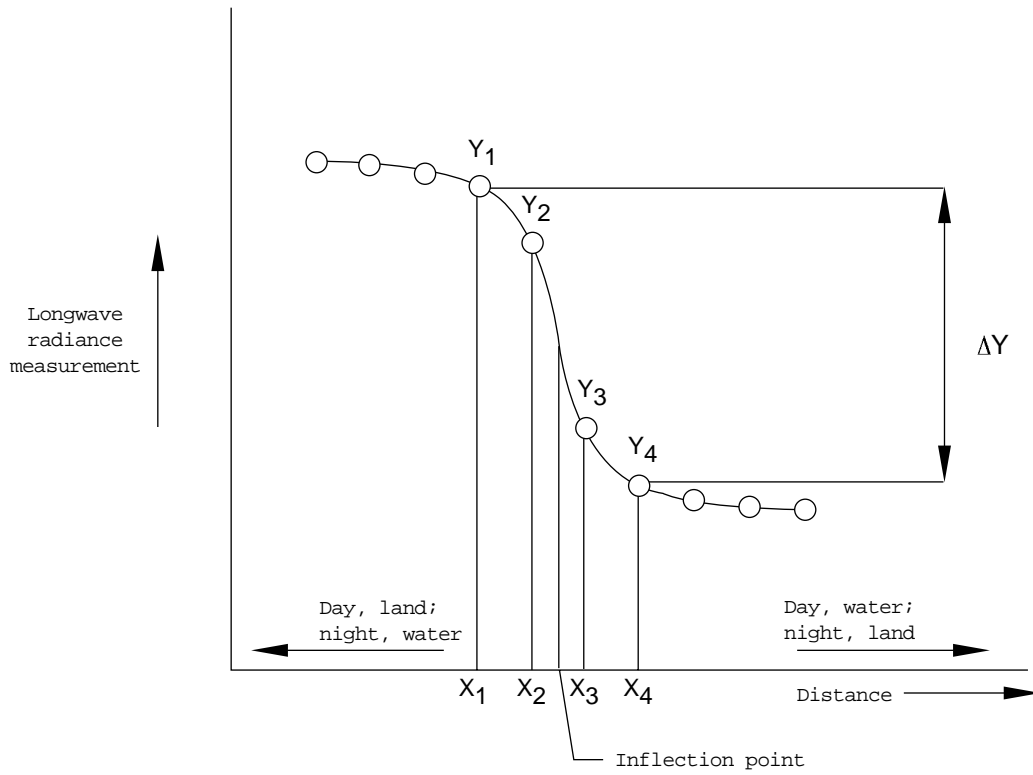
Fig. 7. Sketch of a typical ERBE longwave signal transition obtained when scanning normal to a coastline. The slope of the transition exhibits a diurnal variation. The inflection point was used to represent the location of the coastline.

Satellite:	ERBS
Date:	November 30, 1984
Scan direction:	Left-right
Orbital motion:	Descending
Latitude error:	.0545°
Longitude error:	.0069°
Cross-track error:	-.0478°
Along-track error:	.0271°

Pacific Ocean

○ Coast
□ Spacecraft

Latitude, deg

Longitude, deg E
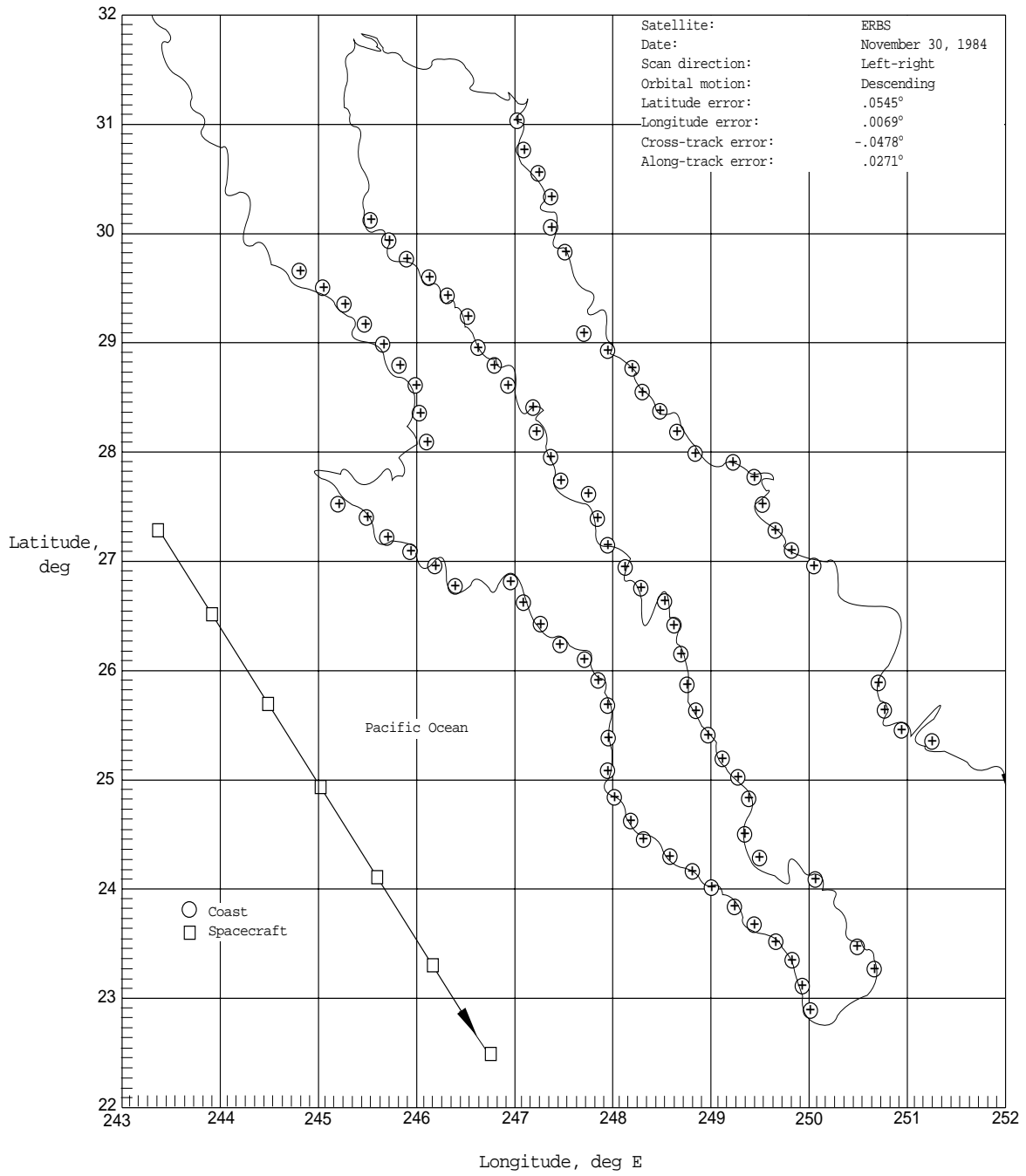
Fig. 8. Plot of the Baja, California coastline overlaid with measured locations of detected coastlines. The ERBS spacecraft sub-satellite point is also indicated in the lower left portion of the plot.
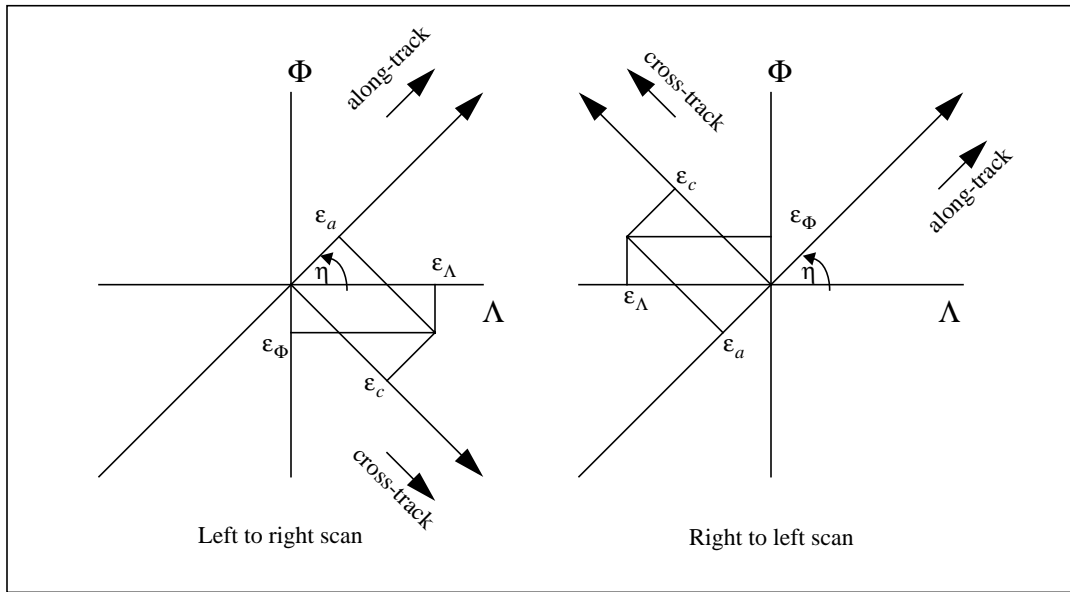
Fig. 9. Transformation from Earth fixed coordinate system to along-track cross-track coordinate.
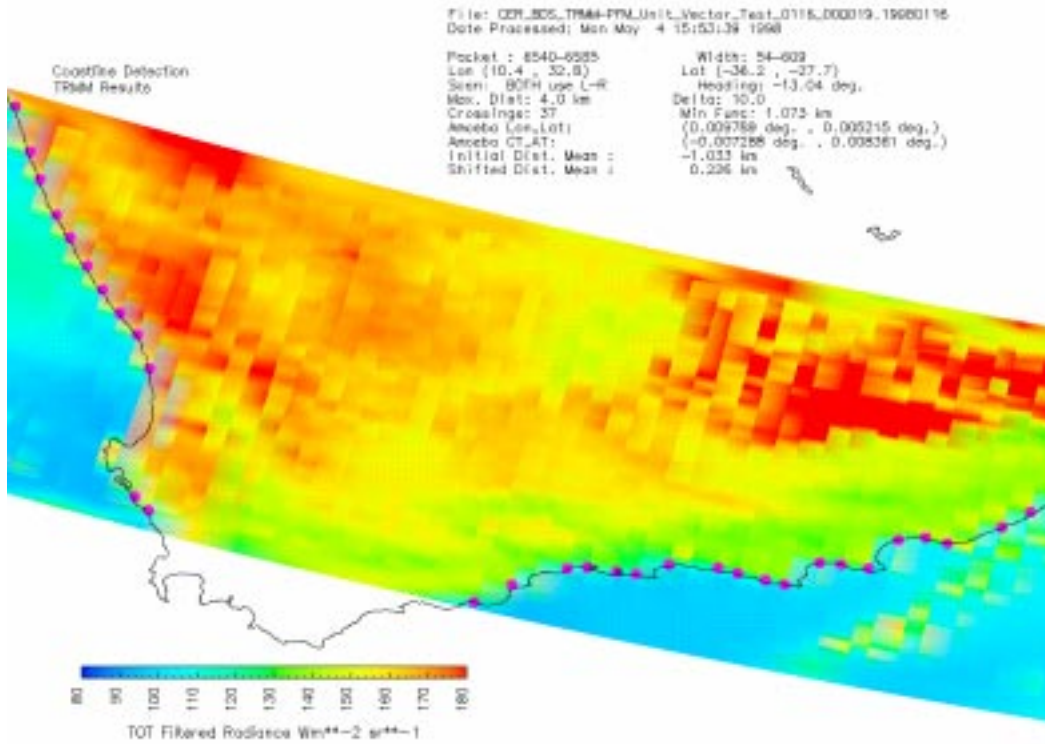
Fig. 10. CERES coastline detection samples collected over South Africa on January 16, 1998.
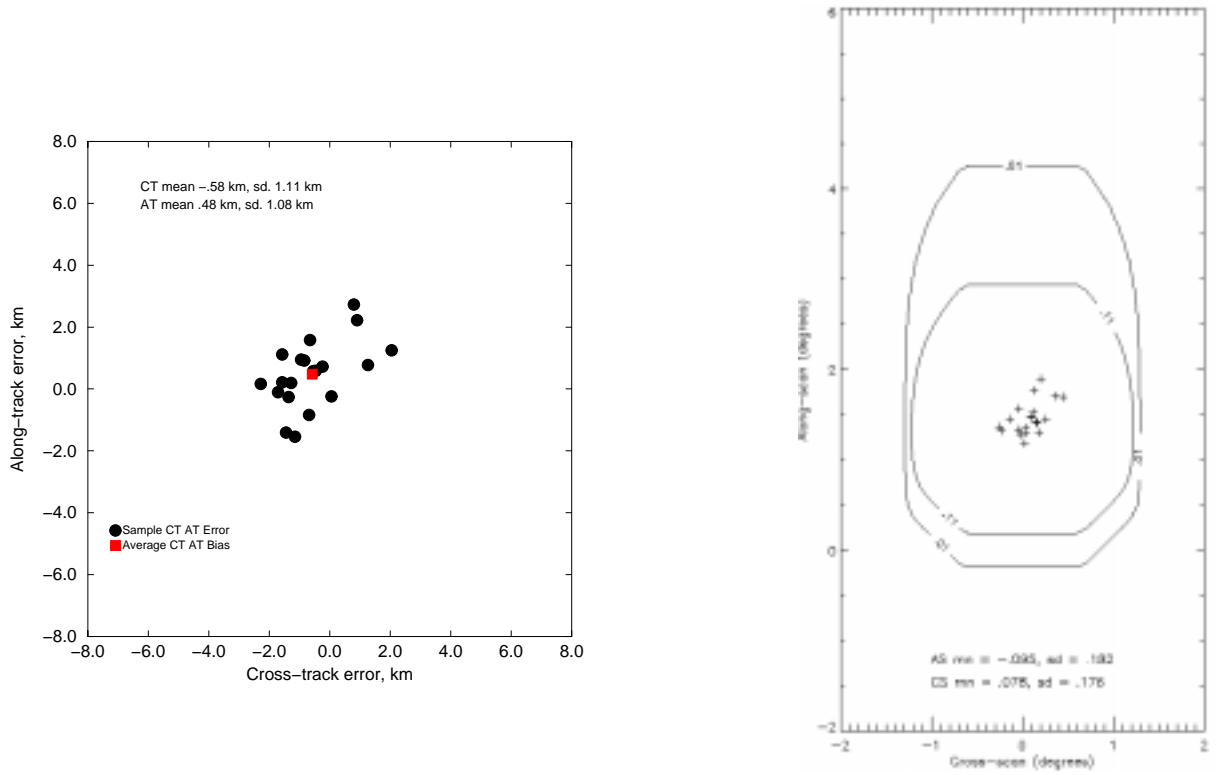
Figure 11. CERES geolocation errors, January 1998, Earth fixed and instrument coordinate systems.

Fig. 11. CERES geolocation errors, January 1998, Earth fixed and instrument coordinate systems.
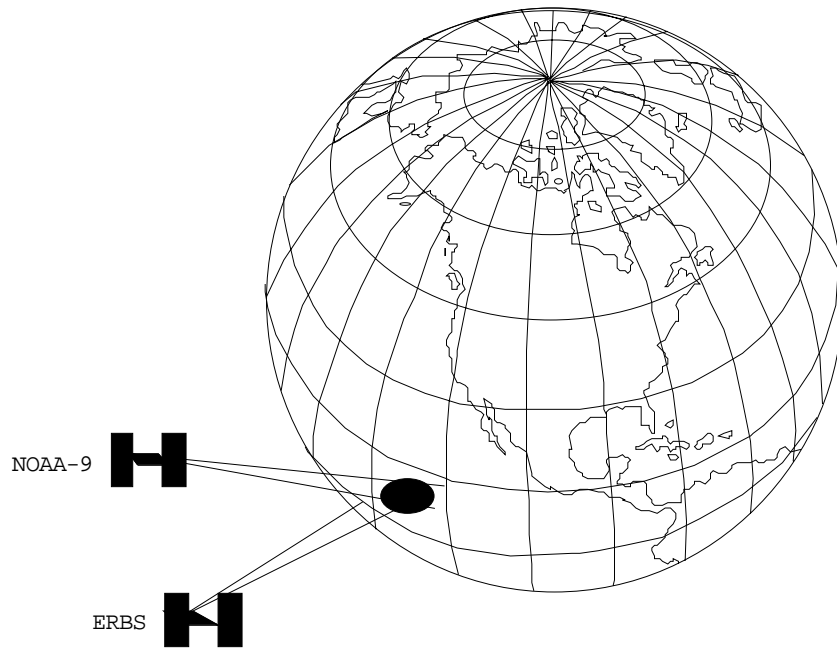
Fig. 12. Geometry for multi-spacecraft radiometric comparisons.
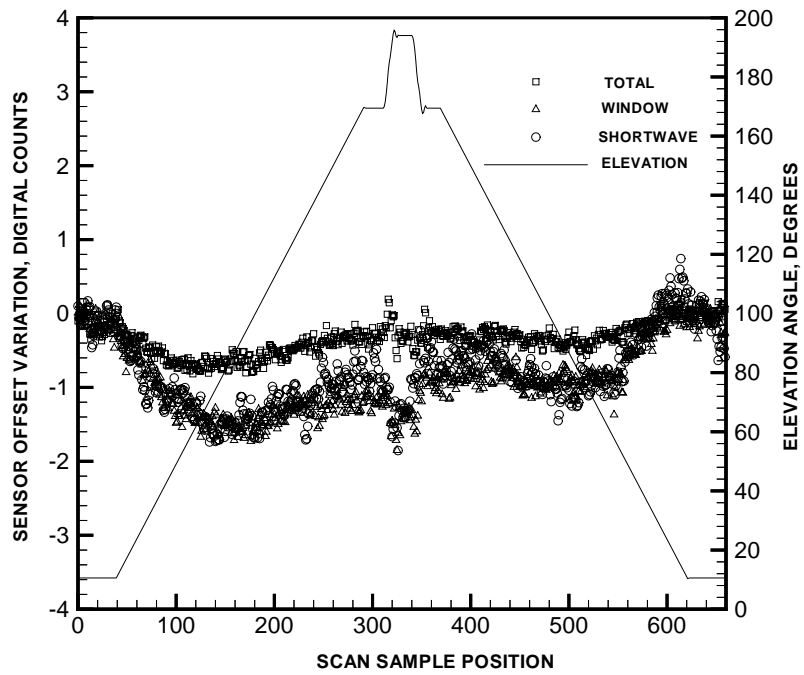
Fig. 13. Variations in the PFM CERES sensors' zero radiance offsets measured with the test caps
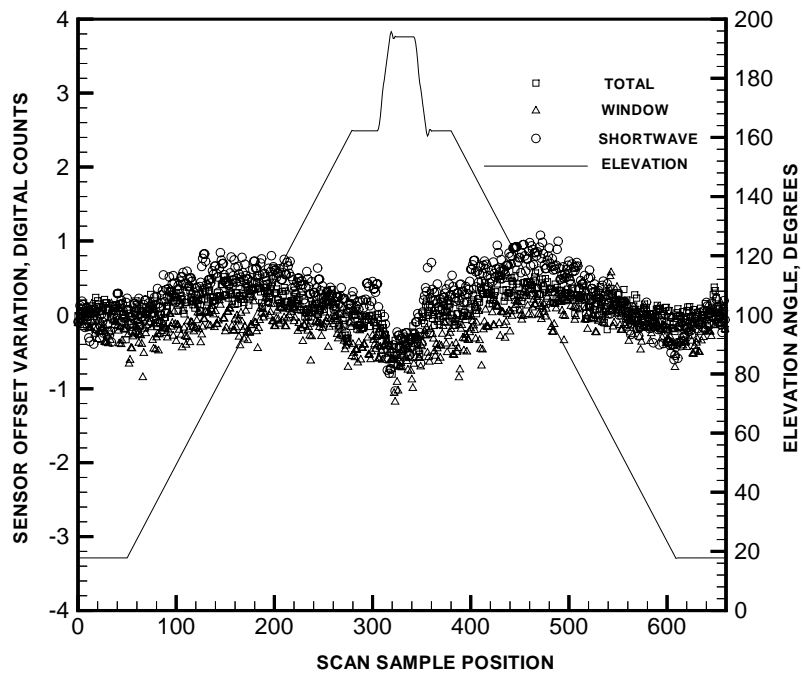
Fig. 14. Variations in the FM1 CERES sensors' zero radiance offsets measured with the test caps
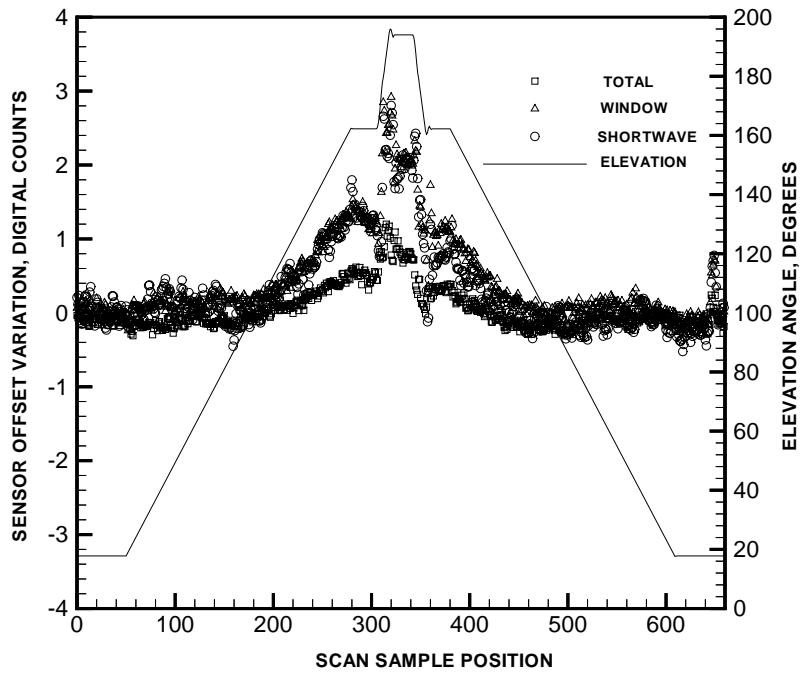
Fig. 15. Variations in the FM2 CERES sensors' zero radiance offsets measured with the test caps

SUN

DAY

EARTH

NIGHT

CROSS-
TRACK
SCAN

CROSS-
TRACK
SCAN

CERES

+Z

BIAXIAL SCAN

EARTH'S SHADOW
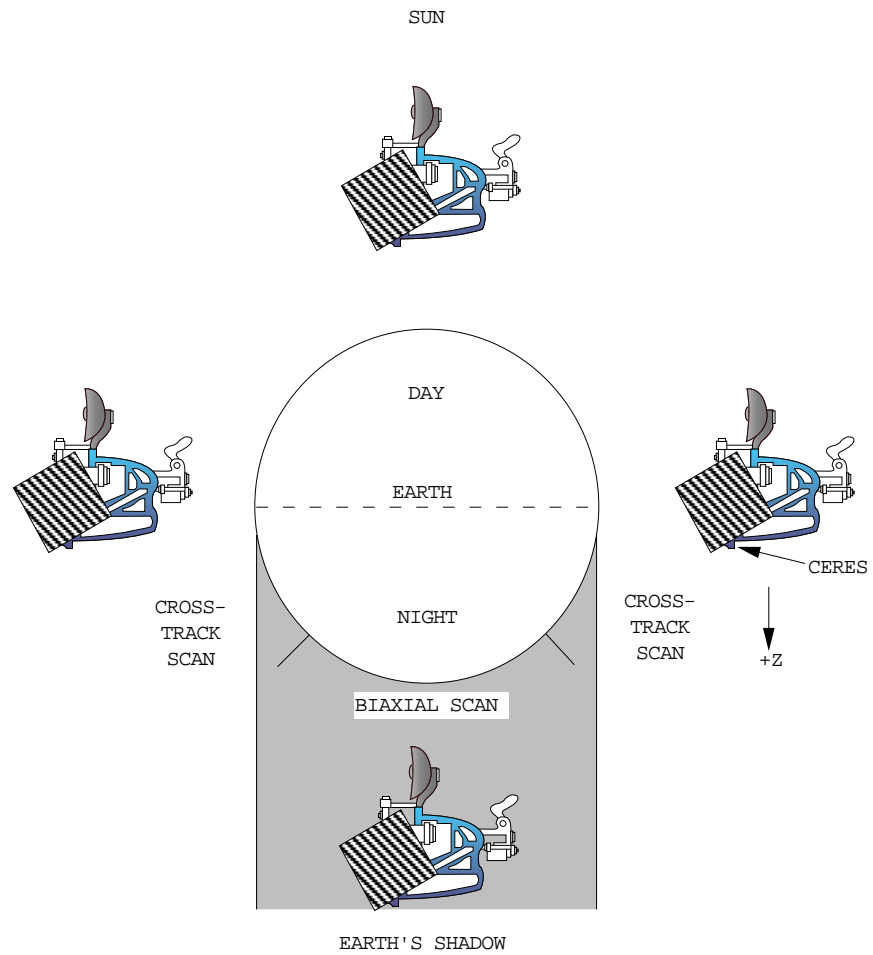
Fig. 16. TRMM Calibration attitude maneuver (CAM) geometry for determining sensor zero-radiance offset variations with elevation scan and azimuth angles.
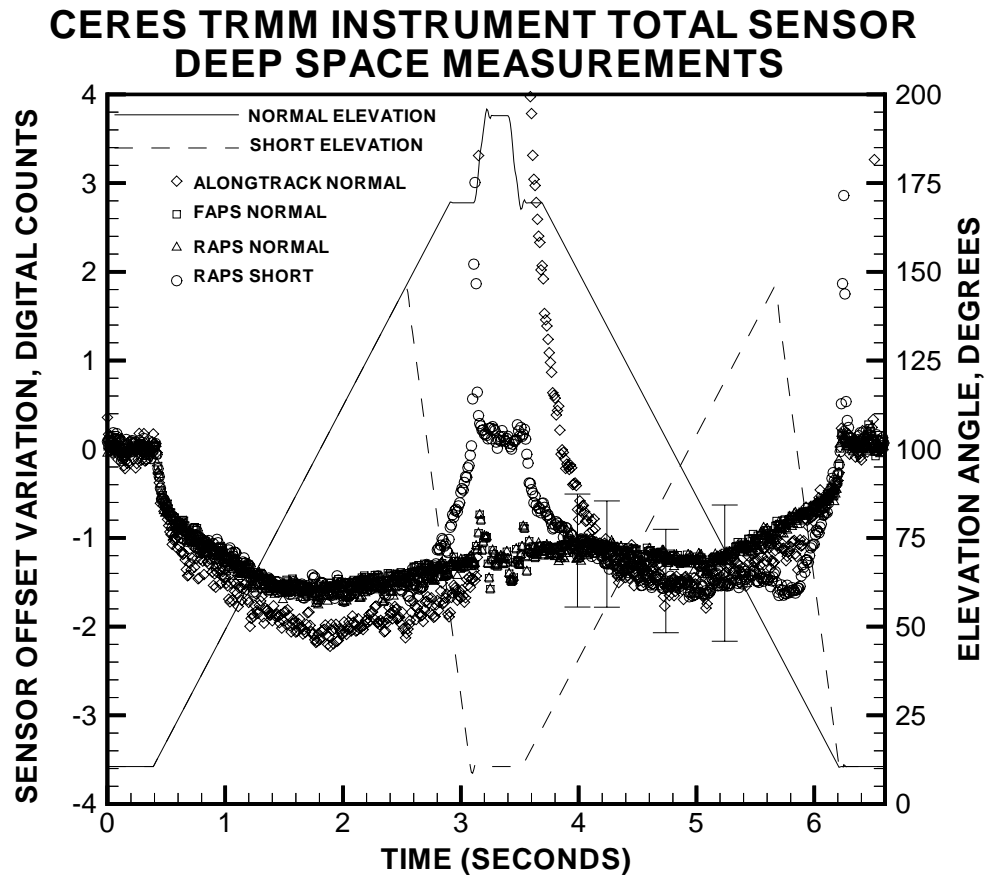
Fig. 17. Variations in the PFM CERES Total sensors' zero radiance offsets measured during deep space maneuver
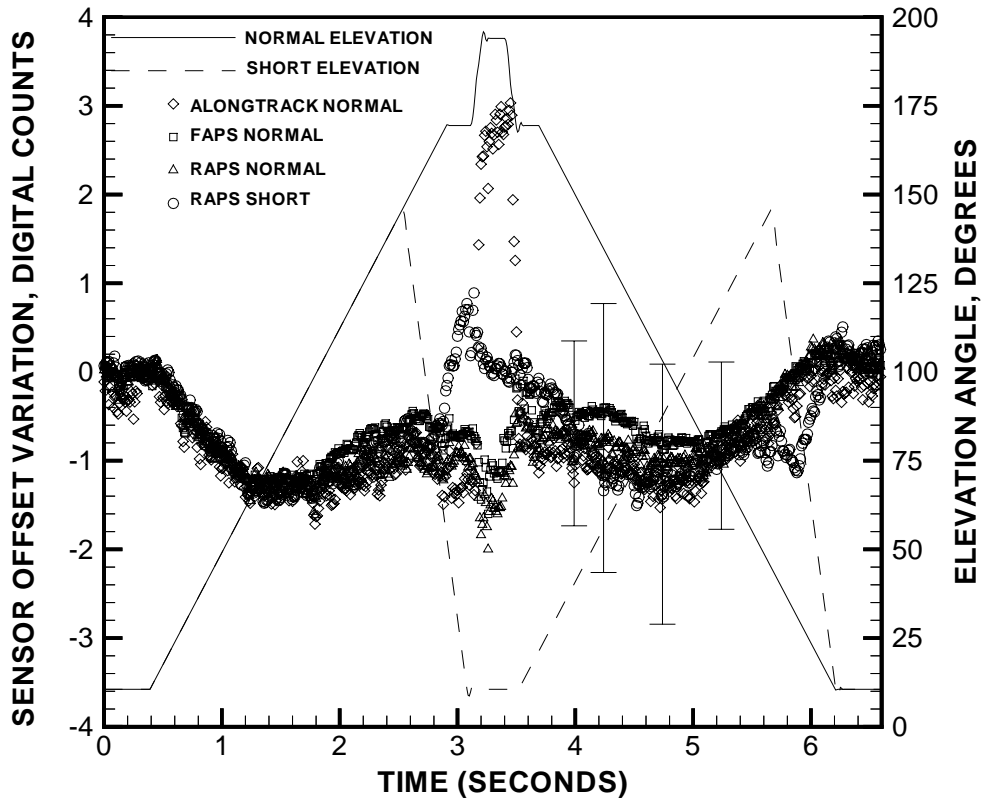
Fig. 18. Variations in the PFM CERES Shortwave sensors' zero radiance offsets measured during deep space maneuver
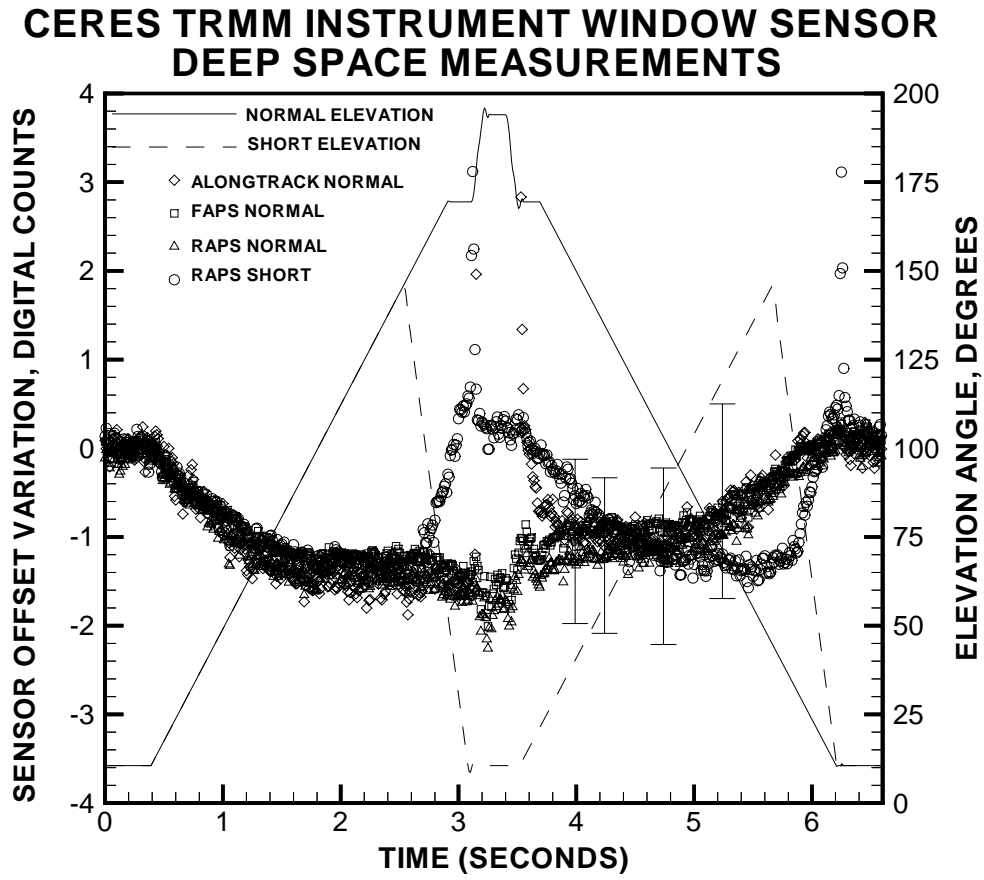
Fig. 19. Variations in the PFM CERES Window sensors' zero radiance offsets measured during deep space maneuver
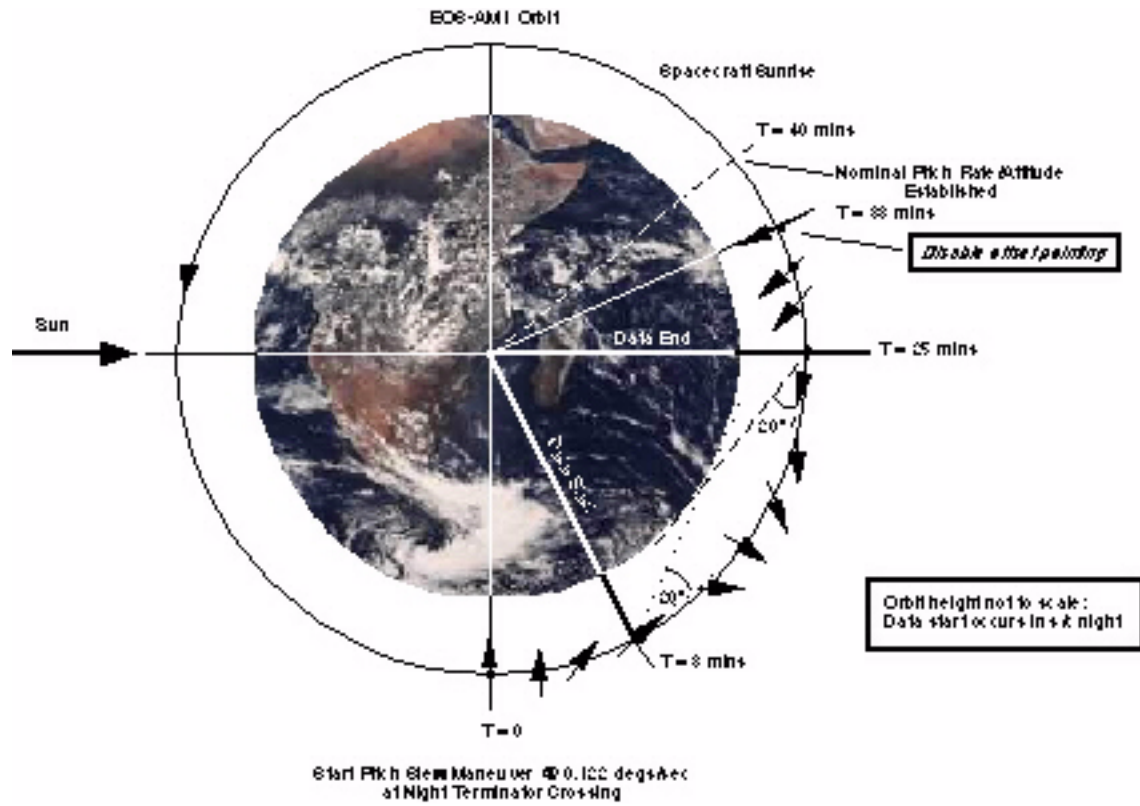
Fig. 20. EOS AM-1 calibration attitude maneuver (CAM) geometry is illustrated in the CERES is scheduled to determine sensor zero-radiance offset variations as functions of elevation scan and azimuth angles.

EOS AM-1 CALIBRATION ATTITUDE MANEUVER (CAM) GEOMETRY FOR CERES SENSOR ZERO-RADIANCE OFFSET VARIATIONS DETERMINATIONS AS FUNCTIONS OF ELEVATION AND AZIMUTH SCAN ANGLES.
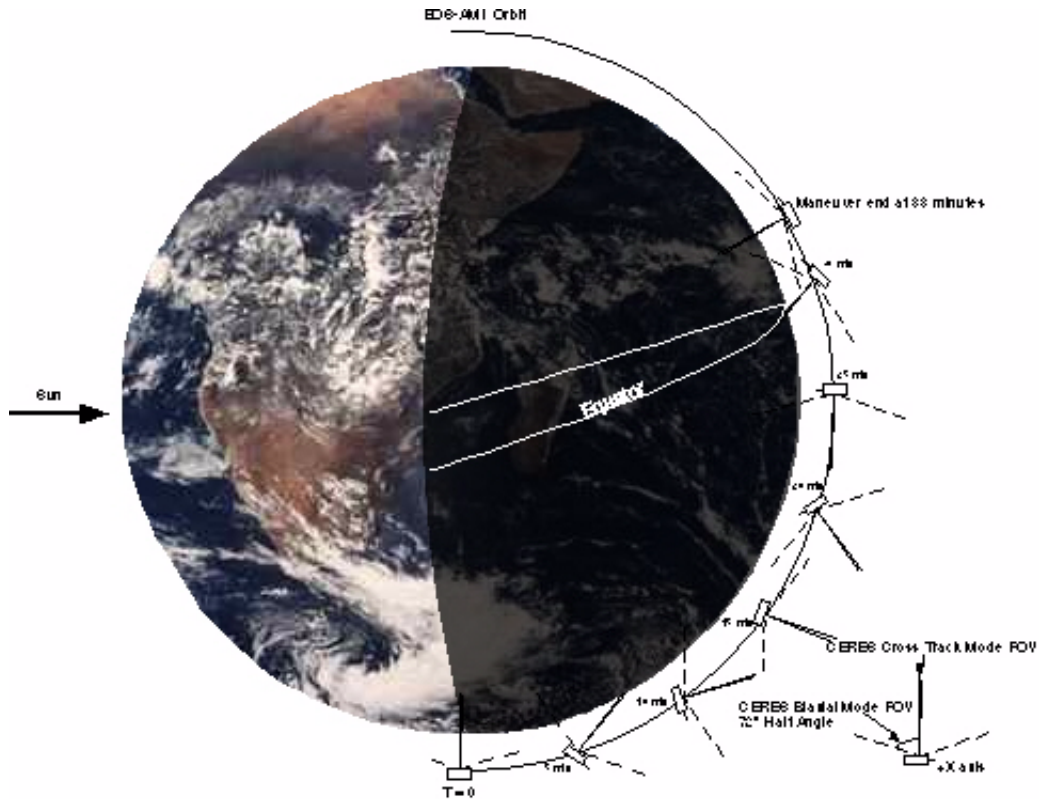

Fig. 21. EOS AM-1 calibration attitude maneuver (CAM) geometry is illustrated for the CERES sensor zero-radiance offset variation deteminations as functions of elevation scan and azimuth angles.

CERES VALIDATION SUMMARY

Subsystem 1.0 - CERES Geolocate and Calibrate Earth Radiances

Data Products

- **Earth radiances:**

    1) **Filtered broadband shortwave [0.3 - 5.0 mm]**

    2) **Total-wave [0.3 - >100 mm]**

    3) **Water vapor window [8 - 12 mm]**

Approach

- **Resolution/geometric sites used during the ERBE spacecraft missions**

- **Radiometric accuracy and precision in-flight calibration systems [demonstrated by ERBE] measurement accuracy via ground-to-orbit and precision via in-flight time series**

- **Radiometric precision/consistency checks among same and different types of CERES sensors using ERBE techniques**

- **Compare CERES radiances to earth validation targets calibrated with 5 years of ERBS data**

- **Three channel redundancy check for consistency**

- **Offsets validated using spacecraft pitch-up and monitored monthly against ERBS global limb-darkening**

CERES VALIDATION SUMMARY

(CONTINUED)

Validation Activities

- **Prelaunch**

    1) All validation and consistency checks will be based upon CERES sensor ground calibration data sets

    2) Establish radiation statistics of earth validation targets. Longwave target is tropical ocean at night. Shortwave target is desert region in daytime. Learn technique by applying to ERBE NOAA-9 data.

- **Postlaunch**

    1) Collection of in-flight calibration measurements and calculated filtered Earth radiances on designated calibration days

    2) Compare CERES radiances to historical ERBS radiances via earth validation targets.

Archive

- **In-flight calibrations will be archived in BDS format at EOSDIS**

- **Publications describing the sensor calibration and validation results as well as public science computing facility (SCF) files of the appropriate calibration and validation data.**

-